Dye Sensitization of Nanocrystalline Titanium Dioxide with Osmium and Ruthenium Polypyridyl Complexes

Geneviève Sauvé, Marion E. Cass,[†] George Coia, Stephen J. Doig, Iver Lauermann,[‡] Katherine E. Pomykal,[§] and Nathan S. Lewis*

Division of Chemistry and Chemical Engineering, 127-72, California Institute of Technology, Pasadena, California 91125

Received: January 14, 2000; In Final Form: April 6, 2000

A series of osmium polypyridyl complexes having various ground-state reduction potentials has been synthesized and used to sensitize nanoporous titanium dioxide electrodes to solar illumination. The spectral response and current vs potential properties of electrodes modified with these dyes have been compared with the behavior of their ruthenium analogues. The trends can be explained by the differences in absorption spectra and ground-state redox potentials. The osmium complexes appear to be promising candidates for further optimization in operating photoelectrochemical cells for solar energy conversion applications. Of the materials studied, all complexes having ground-state redox potentials in methanol more positive than ∼0.4 V vs aqueous SCE were able to sustain oxidation of I^-/I_3^- with a high steady-state quantum yield. For electrodes with very low dye coverages, the open-circuit voltage was mainly determined by the rate of reduction of I_2, whereas for high dye coverages, the open-circuit voltage depended on the nature of the complex and on the dye loading level.

I. Introduction

One approach to the useful conversion of sunlight into electrical energy employs wide band gap semiconductors. These compounds tend to be more stable to oxidation by air and water than small band gap semiconductors such as Si, InP, and GaAs.[1] However, photoelectrodes made from wide band gap materials must be sensitized with dyes or with high concentrations of dopants in order to extend their wavelength responses into the visible region of the solar spectrum. In a particularly exciting development, Grätzel and co-workers have developed efficient photoelectrochemical cells through the use of sensitizers based on transition metal complexes deposited on nanocrystalline titanium dioxide electrodes.[2−4]

The highest efficiency reported to date for such systems has been obtained using nanocrystalline TiO_2 coated with [Ru(II)-(4,4′-$(CO_2H)_2$-2,2′-bipyridine)$_2$$(NCS)_2$] (abbreviated herein as $(Ru(H_2L')_2(NCS)_2)$, where L′ is 4,4′-dicarboxylato-2,2′-bipyridine), for which overall solar-to-electrical energy conversion efficiencies of up to 10% have been reported.[4] The approximate energetics for this system are depicted in Scheme 1. Notably, the $(Ru(H_2L')_2(NCS)_2)$ complex requires excitation by 2.5 eV photons before significant light absorption takes place. In addition, the redox potential of $(Ru(H_2L')_2(NCS)_2)^{+/0}$ is ∼ 0.5 V more positive than the redox potential of the I^-/I_3^- system that is used to carry the faradaic charge in the electrolyte. Consequently, changes in the sensitizer that extend its light absorption to lower energies while maintaining the excited-state redox potential at the same energy level relative to the TiO_2 can yield improved efficiencies, provided that such changes do not produce concomitant decreases in the open-circuit voltage and/or the fill factor of the resulting photoelectrochemical device.

SCHEME 1: Energetics for the Sensitization of Nanocrystalline TiO_2 with [Ru(II)(4,4′-$(CO_2H)_2$-2,2′-bipyridyl)$_2$$(NCS)_2$], Abbreviated $(Ru(H_2L')_2(NCS)_2)$[a]

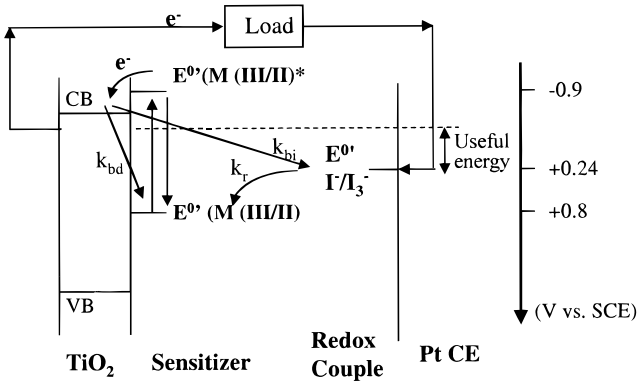

[a] The notation k_{bd} indicates the rate constant for recombination of Ru(III) with electrons in the TiO_2, k_{bi} indicates the rate constant for reduction of oxidized species in the electrolyte by electrons in the TiO_2, and k_r represents the rate constant for production of Ru(II) from the reaction of Ru(III) with electron donor species in the solution.

This strategy has been explored by a few researchers, with limited success to date.[3,5−10] In this work, we explore the approach of replacing ruthenium with osmium in the transition metal complexes that are used to sensitize nanocrystalline TiO_2. The osmium complexes are expected to have an additional absorption band at longer wavelengths compared to a ruthenium complex having the same ligands, because direct excitation to the triplet state in Os(II) $(bipyridyl)_xL_y$ systems is not as forbidden as in the Ru(II) $(bipyridyl)_xL_y$ systems.[11] Higher photocurrents are therefore expected for TiO_2 electrodes coated with the osmium complexes, provided that the excited state in the Os complex effectively injects electrons into the TiO_2 support.

* To whom correspondence is to be addressed.
[†] Carleton College, One North College St., Northfield, MN 55057.
[‡] Hahn-Meitner-Institut, Glienicker Str. 100, Berlin D-14109, Germany.
[§] Eveready Battery Company, 25225 Detroit Rd., Westlake, OH 44145.

10.1021/jp0002143 CCC: $19.00
Published on Web 06/30/2000

CHART 1: Hydrogen Numbering for the ^{1}H NMR Assignment of the Dye Complexes (X = NCS^-, CN^- or Cl^-; M Is Os or Ru; H_2L Is 4,4′-$(CO_2H)_2$-2,2′-bipyridyl; L Is 2,2′-bipyridyl)

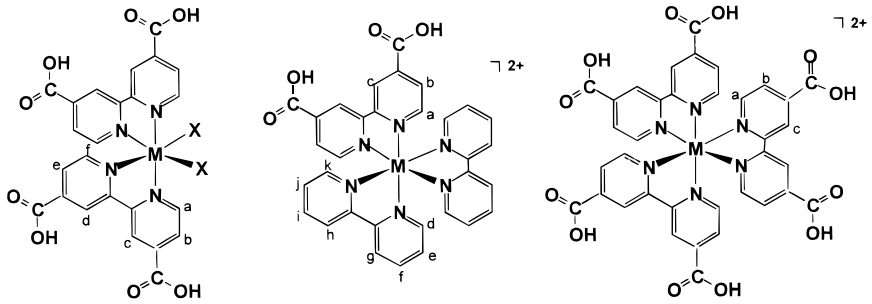

The Os complexes have other potential advantages relative to their Ru analogues. Although the excited-state lifetimes for Os complexes are typically shorter than those for the analogous Ru complexes, the Os(II) excited state should be as effective as the Ru(II) species in sensitizing TiO_2 because electron injection into nanocrystalline TiO_2 is thought to occur on a subpicosecond time scale.[12−16] Perhaps more importantly, the ground-state potential of the Os complexes can be readily tuned to less positive potentials by using stronger donor ligands.[17] By using a sensitizer with a less positive ground state redox potential and a constant excited-state redox potential, less energy will be wasted in the reduction of Os(III) to Os(II) by I_3^-/I^-, possibly yielding even further improvements in the efficiency of the overall system. However, it is not clear whether the ground states of the Os(III) dyes will have sufficient driving force to oxidize I_3^-/I^- at a rate rapid enough to support the required current density between the electrodes in the cell under typical solar illumination conditions. We have therefore performed electrochemical experiments to determine both the ground and excited-state redox potentials of the Os and Ru complexes in order to probe the device performance as a function of the position of these energetic parameters.

Finally, if the dominant back reaction in all cases is reduction of I_2, as has been proposed to be the rate-determining process in the specific case of $Ru(H_2L')_2(NCS)_2$ as the sensitizer for nanocrystalline TiO_2 electrodes,[4] one would expect that the photovoltage would remain relatively constant at a constant carrier injection level, regardless of which dye is used to generate the injected electrons into the TiO_2 support. Use of a series of dyes (Chart 1) has allowed us to probe the generality of this hypothesis in order to better understand the factors that control the photovoltage of dye-sensitized nanocrystalline TiO_2/CH_3CN contacts.

II. Experimental Section

A. Materials. $(NH_4)_2[OsCl_6]$ (Alfa, 99.99%), 2,2′-bipyridine-4,4′-dicarboxylic acid (Alfa), 2,2′-bipyridine (Aldrich, 99%+), HPF_6 (Aldrich), NaCN (EM Science), NaSCN (Alfa), $Na_2S_2O_4$ (Alfa), $KS^{13}C^{15}N$ (Isotech), $K^{15}NO_3$ (Isotech), CF_3SO_3H (Aldrich), D_2O with 1% w/w 3-(trimethylsilyl)-1-propanesulfonic acid, sodium salt (DSS) (Aldrich), d^6-DMSO (CIL), ethylene glycol (EM Science), Sephadex LH-20 (Fluka), and Sephadex DEAE A-25 (Aldrich) were used without further purification. Lithium iodide (Alfa, 99%, anhydrous) was used as received but was stored in a drybox until use. Iodine (Aldrich, 99.99%+) was sublimed under vacuum before use. Pyridinium triflate was purified by dissolving the material obtained from the vendor (97%, Aldrich) into a minimum amount of warm acetonitrile, and the salt was then precipitated by addition of diethyl ether. The precipitate was filtered through a medium-porosity glass frit and was washed with ether and then dried overnight under vacuum. Pyridine (J. T. Baker) was distilled before use. Anhydrous lithium perchlorate (J. T. Baker) was dried at 180 °C for 48 h under active vacuum. All solvents used were reagent grade (EM Science) except for absolute ethanol, which was purchased from Quantum Chemicals. Acetonitrile was predried over CaH_2 and distilled over P_2O_5. 17.8 MΩ cm resistivity water was obtained from a Barnstead Inc. NANOpure filtration system.

Syntheses of the Complexes. *cis*-$[OsL_2Cl_2]$:*cis*-Bis(2,2′-bipyridyl)dichloroosmium(II). OsL_2Cl_2 (L = 2,2′-bipyridyl) was synthesized following the procedure of Kober et al.[18] $[OsCl_6](NH_4)_2$ (0.384 g, 8.7×10^{-4} mol) and 2,2′-bipyridine (0.277 g, 1.77×10^{-3} mol) were first dissolved in 20 mL of ethylene glycol in a 100 mL round-bottom Schlenk flask. The mixture was then heated to 170 °C for 2 h with stirring, under nitrogen. After this time, sodium dithionite (0.4 g, 2.2×10^{-3} moles) was dissolved in 20 mL of water and added dropwise to the cooled mixture while stirring, to convert excess Os(III) to Os(II). The dark purple precipitate was filtered, washed with water to remove ionic products and $[OsL_3]^{2+}$, and washed with ether to remove unreacted ligand. The final product was dried under vacuum overnight. Yield: 0.43 g.

$[OsL_2(H_2L')](PF_6)_2$: Bis(2,2′-bipyridyl)(4,4′-dicarboxy-2,2′-bipyridyl)-osmium(II) hexafluorophosphate. $[OsL_2(H_2L')](PF_6)_2$ (L′ = 4,4′-dicarboxylato-2,2′-bipyridine) was prepared as follows: $NaHCO_3$ (0.222 g, 2.65×10^{-3} mol) and 2,2′-bipyridine-4,4′-dicarboxylic acid (0.213 g, 8.72×10^{-4} mol) were dissolved in 15 mL of water. This mixture was added to 0.427 g (7.4×10^{-4} mol) of OsL_2Cl_2 dissolved in 15 mL of ethanol, and the solution was refluxed with stirring for 6 h under nitrogen. NH_4PF_6 (0.3 g, 1.8×10^{-3} moles) was dissolved in 5 mL of water and was then added to the cooled reaction mixture. The ethanol was evaporated using a rotary evaporator and 10 drops of 0.25 M HPF_6 were added to precipitate $[OsL_2(H_2L')](PF_6)_2$. The resulting mixture was left in the refrigerator overnight. The black precipitate was filtered, washed with pH 1.5 water (acidified with HPF_6) and with ether, and dried overnight under vacuum. A parent ion was observed at 748 amu in the fast atom bombardment mass spectrum (FAB/MS) (mass expected for $[OsL_2(H_2L')](PF_6)^+$ is 748 amu), and another peak, ascribed to $[OsL_2(H_2L')](PF_6)_2^+$, was observed at 893 amu. The product was dissolved in a minimum amount of 0.1 M $NaHCO_3$ (aq) and loaded onto a chromatography column (2.5 cm diameter) that had been packed with approximately 30 cm of anion-exchange resin (Sephadex DEAE A-25 in water). The eluent was pure water, and the first band (green) was discarded. The second band (brown, major band) was collected and the volume reduced to 5−10 mL by rotary evaporation. The product was precipitated upon addition of 1.0 M HPF_6 (aq), filtered with a fine-porosity glass frit and washed with 0.1 M HPF_6 (aq) and diethyl ether. The solid was then dried under vacuum overnight. Elemental analysis for $C_{32}H_{24}N_6O_4P_2F_{12}Os \cdot 6H_2O$ gave (calcu-

lated values in parentheses) C, 33.46 (33.57); H, 2.80 (3.17); N, 7.22 (7.34). The chloride salt was isolated by taking the eluted band from the ion exchange column, adding a minimum amount of 1.0 M HCl and evaporating to dryness using a rotary evaporator. Elemental analysis for $C_{32}H_{24}N_6O_4Cl_2Os\cdot 6H_2O$ gave (calculated values in parentheses) C, 41.44 (41.52); H, 4.26 (3.92); N, 9.18 (9.08).

$K_4[OsL'_3]$: Tetrapotassium tris(4,4′-dicarboxylato-2,2′-bipyridyl)osmiate(II)**.** $[OsCl_6](NH_4)_2$ (0.171 g, 3.90×10^{-4} mol), H_2L' (0.2942 g, 1.20×10^{-3} mol), and a few drops of 1.0 M NaOH (aq) were mixed in 25 mL of ethylene glycol and heated to 190 °C for 2 h with stirring under nitrogen. The mixture was transferred to a large beaker and 125 mL of water was added. 0.25 M HPF_6 (aq) was added dropwise until the pH was 1.5 to 2 and a large excess of KPF_6 (1 g, 5×10^{-3} mol) was then added in order to precipitate the product. The dark green precipitate was filtered with a fine-porosity glass frit and washed with 0.1 M HPF_6 and ether. The FAB/MS parent ion was observed at 924.1 (expected at 924.1 for $[Os(H_2L')_3(PF_6)_2]^+$). $[Os(H_2L')_3](PF_6)_2$ was then dissolved in 0.2 M KOH (aq) and purified by ion exchange column chromatography using Sephadex DEAE A-25 as the column support. Impurities were eluted with water and 0.2 M KI. The major green-brown band was eluted with 0.4 M KI (aq), collected and evaporated to dryness using a rotary evaporator. The KI was removed by extraction with absolute ethanol until some of the product dissolved. The remaining KI was removed by extraction with acetone, and $K_4[OsL'_3]$ was isolated by filtration. $K_4[OsL'_3]$ was dissolved in methanol, precipitated upon addition of acetone, filtered, and washed with acetone and ether. The solid was dried under vacuum overnight. Elemental analysis for $C_{36}H_{18}N_6O_{12}K_4Os\cdot 6H_2O$ gave (calculated values in parentheses) C, 36.70 (36.54); H, 2.60 (2.73); N, 6.97 (7.10). The chloride salt of the fully protonated complex was obtained by dissolving $K_4[OsL'_3]$ in a few milliliters of water, adding 1 M HCl to precipitate the chloride salt, and filtering with a fine-porosity glass frit. Elemental analysis for $C_{36}H_{24}N_6O_{12}Cl_2Os\cdot 6H_2O$ gave (calculated values in parentheses) C, 39.49 (39.24); H, 3.37 (3.29); N, 7.54 (7.63).

cis-$[Os(H_2L')_2Cl_2]$: *cis*-Dichlorobis(4,4′-dicarboxy-2,2′-bipyridyl)osmium(II). The synthesis of $Os(H_2L')Cl_2$ was adapted from the procedure of Heimer et al.[5] $[OsCl_6](NH_4)_2$ (0.1950 g, 4.44×10^{-4} mol) and H_2L' (0.190 g, 7.78×10^{-4} mol) were heated at 170 °C for 2 h in 30 mL of ethylene glycol under nitrogen. The mixture was then transferred into a large beaker and diluted with 150 mL of water. $Na_2S_2O_4$ (0.1 g, 6×10^{-4} mol) was added to reduce any Os(III) to Os(II). The dark purple precipitate was isolated by centrifugation. Purification consisted of dissolving the product in water with a minimum amount of NaOH (aq), precipitating the solid with 2 M HCl (aq), and isolating the precipitate by centrifugation. The product was dissolved in acetone and filtered to remove unreacted ligand (H_2L') (which is insoluble in acetone). Approximately 20 mL of pH 2 water (acidified with HCl) were added to the solution and the product was precipitated by evaporation of the acetone under vacuum. The precipitate was isolated by centrifugation, washed twice with pH 2 water (acidified with HCl), and then dried overnight under vacuum. The yield was 55%. This complex is readily oxidized in air and was therefore kept under an inert atmosphere. A FAB/MS parent ion peak was observed at 749 amu (expected at 750 amu for $[Os(H_2L')_2Cl_2]^+$) presumably reflecting the loss of one proton from the fully protonated complex.

cis-$Os(H_2L')_2(CN)_2$:*cis*-Dicyanobis(4,4′-dicarboxy-2,2′-bipyridine)osmium(II). This synthesis is adapted from the procedure reported by Heimer and al.[5] $Os(H_2L')_2Cl_2$ (0.084 g, 1.1×10^{-4} mol) was dissolved with KCN (0.27 g, 4.1×10^{-3} mol) in 7 mL of water and the solution was refluxed for 12 h with stirring under a nitrogen atmosphere. The cooled reaction mixture was poured into 100 mL of N,N′-dimethylformamide, DMF, to precipitate $K_4[OsL'_2(CN)_2]$. The brown precipitate was isolated by filtration, washed with DMF and acetone, and dried under vacuum overnight. The crude product was dissolved in water and purified by column chromatography using Sephadex DEAE A-25 as the column support and 0.5 M KNO_3 (aq) as the eluent. The major band (green-brown) was collected. The mixture was evaporated to about 100 mL and filtered to remove excess KNO_3. The filtrate was further evaporated to 20 mL and filtered to remove additional KNO_3. One milliliter of 0.26 M CF_3SO_3H (aq) was added to the filtrate to precipitate the desired complex, which was isolated by filtration, washed with 0.26 M CF_3SO_3H (aq) and ether, and then dried under vacuum overnight. This complex produced a parent ion peak at 730.9 (expected at 731 for $[^{192}Os(H_2L')_2(CN)_2]^-$ in an electrospray mass spectrometer operated in negative ion mode. In addition, the isotope pattern around this parent mass peak agreed with the calculated isotope pattern for $Os(H_2L')_2(CN)_2$.

cis-$[Os(H_2L')_2(NCS)_2]$: *cis*-Bis(4,4′-dicarboxy-2,2′-bipyridyl)-bis(isothiocyanato)osmium(II). This preparation was adapted from the published synthesis of $OsL_2(NCS)_2$.[19] $Os(H_2L')_2Cl_2$ (0.16 g, 2×10^{-4} mol), NaSCN (0.8 g, 1×10^{-2} mol), and 1 mL of 1.0 M NaOH (aq) were mixed with 15 mL of water and refluxed for 5 h under nitrogen. HCl (aq) (1.0 M, 2.5 mL) was then added to precipitate the product. The mixture was left overnight in the refrigerator. The product was filtered and washed with 0.1 M HCl (aq). The product was dissolved in a minimum amount of methanol and purified by column chromatography using Sephadex LH-20 as the column support and methanol as the eluent. The first band (brown-green) was likely due to $Os(H_2L')_3^{2+}$ and was discarded. Other, orange-colored, bands that eluted quickly were also discarded. The main band, which was dark purple and eluted very slowly, eventually becoming very wide, was collected. The methanol was evaporated from the collected fraction using a rotary evaporator, and the final product was dried overnight under vacuum. Elemental analysis for $C_{26}H_{16}N_6O_8S_2Os\cdot 5H_2O$ gave (calculated values in parentheses) C, 35.23 (35.29); H, 2.63 (2.96); N, 9.37 (9.50).

cis-$[Os(H_2L')_2(^{15}N^{13}CS)_2]$: *cis*-Bis(4,4′-dicarboxy-2,2′-bipyridyl)bis(^{15}N, ^{13}C-isothiocyanato)osmium(II). The ^{15}N, ^{13}C labeled sample of the isothiocyanato complex was synthesized by a slightly different procedure. $Os(H_2L')_2Cl_2$ (0.0660 g, 8.81×10^{-5} mol) and $KS^{13}C^{15}N$ (0.0776 g, 7.82×10^{-4} mol) were dissolved in 4 mL of H_2O and 352 μL of 1.0 M KOH (aq). The reaction flask was purged with argon and the reaction refluxed under a positive pressure of argon for 8 h. The product was precipitated with 2 mL of 0.267 M CF_3SO_3H (aq), then centrifuged and the filtrate removed. Twice, the product was redissolved in 350 μL of 1.0 M KOH (aq), precipitated with 2 mL of 0.267 M CF_3SO_3H (aq), centrifuged, and the filtrate removed. The product was then dried in a vacuum desiccator. The FAB/MS of the complex made through an analogous synthesis, but using unlabeled KSCN, yielded a parent ion peak M^+ at 796 amu (expected 796 amu) and an infrared peak at 2111 cm^{-1} (ascribed to the C≡N stretch in M-NCS).

cis-$[Ru(H_2L')_2Cl_2]$: *cis*-Dichlorobis(4,4′-dicarboxy-2,2′-bipyridyl)ruthenium(II). $RuCl_3\cdot 3H_2O$ (0.13 g, 5.0×10^{-4} mol) and H_2L' (0.24 g, 1.0×10^{-3} mol) were dissolved in 15 mL of ethylene glycol, and the solution was purged with argon.[20] The

solution was then stirred for 2 h at 150 °C under argon, and the ethylene glycol removed by distillation under vacuum at 80 °C. The product was then dissolved in ~100 mL of methanol and 20 drops of 1 M HCl (aq) were added. The mixture was filtered to remove unreacted ligands and the methanol was evaporated from the filtrate using a rotary evaporator. The product was then redissolved in ~1 mL of 1 M NaOH (aq) and precipitated by addition of 1 mL of 1 M HCl (aq). The final product was cooled in an ice bath for a few hours, filtered, washed with 100 mL of 0.1 M HCl (aq) followed by 30 mL of ether, and dried overnight under vacuum.

cis-[$Ru(H_2L')_2(NCS)_2$]: *cis*-Bis(4,4′-dicarboxy-2,2′-bipyridyl)-bis(isothiocyanato)ruthenium(II). $Ru(H_2L')_2Cl_2$ (0.1 g, 1.7×10^{-4} mol) and NaSCN (0.35 g, 4.3×10^{-3} mol) were dissolved in 5 mL of water and 1 mL of 1.0 M NaOH (aq). The mixture was stirred at reflux under nitrogen for 22 h. After cooling the mixture, ~2 mL of 1.0 M HCl (aq) was slowly added to precipitate the product. The mixture was then left overnight in an ice bath. The product was isolated by vacuum filtration, washed with 0.1 M HCl (aq) and with ether, and dried overnight under vacuum. The dried product contained an impurity, likely $Ru(H_2L')_3$, as seen by emission spectroscopy. This product was therefore further purified by column chromatography using LH-20 as the column support and methanol as the eluent. The first band (orange) was attributed to $Ru(H_2L')_3^{2+}$ and was discarded. The second band (dark red-purple) was collected. The methanol was evaporated using a rotary evaporator and the product dried overnight under vacuum. Because the $Ru(H_2L')_3^{+2}$ and $Ru(H_2L')_2(NCS)_2$ bands eluting from the column overlapped slightly, the purification by column chromatography was repeated a second time. After the second purification, the emission spectrum showed no evidence of $Ru(H_2L')_3^{2+}$ in the product. Elemental analysis for $C_{26}H_{16}N_6O_8S_2Ru \cdot 3H_2O$ gave (calculated values in parentheses) C, 41.16 (41.11); H, 2.67 (2.92); N, 10.85 (11.06).

cis-[$Ru(H_2L')_2(^{15}N^{13}CS)_2$]: *cis*-Bis(4,4′-dicarboxy-2,2′-bipyridyl)bis(^{15}N, ^{13}C-isothiocyanato)ruthenium(II). The ^{15}N, ^{13}C labeled sample of the isothiocyanato complex was synthesized by a slightly different procedure. $RuL'_2(ox)$ (ox = oxalate) was first synthesized by heating in a boiling water bath $K_4[Cl_5Ru-O-RuCl_5] \cdot H_2O$ (0.545 g, 7.47×10^{-4} mol) and $K_2C_2O_4 \cdot H_2O$ (0.825 g, 4.48×10^{-3} mol) in 12 mL of water with stirring under an argon atmosphere. After 3 h, 20 mL of methanol and a solution of 2,2′-bipyridine-4,4′-dicarboxylic acid (0.365 g, 1.495×10^{-3} moles) in 5 mL of water and 5 mL of 1.0 M KOH (aq) were added to the reaction mixture and heated for an additional 8 h. After cooling, the methanol was removed in vacuo and $Ru(H_2L')_2(ox)$ was precipitated upon addition of 0.27 M CF_3SO_3H (aq). The precipitate was isolated by centrifugation. The precipitate was dissolved in a minimum amount of 1.0 M KOH (aq), the solid was precipitated with CF_3SO_3H (aq), and the product was isolated by centrifugation. This process was repeated 2−3 times to remove some impurities. The product was then dried under vacuum overnight. To make $Ru(H_2L')_2(^{15}N^{13}CS)_2$, $Ru(H_2L')_2(ox)$ (0.0590 g, 8.71×10^{-5} mol) and $KS^{13}C^{15}N$ (0.0814 g, 8.20×10^{-4} mol) were dissolved in 4 mL H_2O and 348 μL of 1.0 M KOH (aq). The reaction flask was purged with argon and the reaction refluxed under a positive pressure of argon for 9 h. The product was precipitated with 1.5 mL of 0.267 M CF_3SO_3H (aq), then centrifuged and the filtrate removed. The product was redissolved in 500 μL of 1.0 M KOH (aq), precipitated with 1.5 mL of 0.267 M CF_3SO_3H (aq), centrifuged, and the supernatant removed. The product was dried in a vacuum desiccator.

cis-[$RuL_2(^{15}N^{13}CS)_2$]: *cis*-Bis(2,2′-bipyridyl)bis(^{15}N,^{13}C-isothiocyanato)ruthenium(II). [RuL_2CO_3] was synthesized using a previously reported procedure.[18] [RuL_2CO_3] (0.0600 g, 1.27×10^{-4} mol) and $KS^{13}C^{15}N$ (0.0896 g, 9.03×10^{-4} mol) were then dissolved in 4 mL of absolute ethanol. The reaction mixture was refluxed for 8 h under a positive pressure of argon. The product precipitated from the reaction mixture and was washed with two portions of ethanol to remove excess starting materials. The product was dried in a vacuum desiccator.

cis-[$Ru(H_2L')_2(CN)_2$]: *cis*-Dicyanobis(4,4′-dicarboxy-2,2′-bipyridyl)ruthenium(II). $Ru(H_2L')_2Cl_2$ (0.13 g, 2.3×10^{-4} mol) and NaCN (0.25 g, 5.1×10^{-3} mol) were added to 10 mL of water and the mixture refluxed under nitrogen for 5 h. With caution, 1.0 M HCl (aq) was then added to the cooled mixture to precipitate the product. The dark solid was isolated by centrifugation, washed with 1.0 M HCl (aq), and dried overnight under vacuum. The product was then dissolved in 3 mL of methanol and purified by column chromatography using Sephadex LH-20 as the column support and methanol as the eluent. The first band (orange) was attributed to $Ru(H_2L')_3^{2+}$ and was therefore discarded. The second band (dark brown) was collected, the methanol was evaporated using a rotary evaporator, and the product dried. The solid was then dissolved in 1.5 mL of 0.1 M $NaHCO_3/Na_2CO_3$ (aq) buffer, and addition of 500 μL of 1.0 M HCl (aq) precipitated the product. Water (1.5 mL) and a drop of concentrated HCl were added to the mixture and the solution left overnight in the refrigerator to complete the precipitation. The product was filtered with a fine-porosity glass frit, washed with 0.1 M HCl (aq), and dried overnight under vacuum. Elemental analysis for $C_{26}H_{16}N_6O_8Ru \cdot 3H_2O$ gave (calculated values in parentheses) C, 44.07 (43.76); H, 3.09 (3.39); N, 11.59 (11.78).

[$RuL_2(H_2L')](PF_6)_2$: Bis(2,2′-bipyridyl)(4,4′-dicarboxy-2,2′-bipyridyl)ruthenium(II) hexafluorophospate. [$RuL_2(H_2L')](PF_6)_2$ was prepared by the procedure of Sprintschnik et al.[21] 2,2′-bipyridine-4,4′-dicarboxylic acid (0.153 g, 6.26×10^{-4} mol), $RuL_2Cl_2 \cdot 2H_2O$ (0.26 g, 5.0×10^{-4} mol), and $NaHCO_3$ (0.15 g, 1.8×10^{-3} mol) were dissolved in 5 mL of methanol and 7.5 mL of H_2O. The reaction was stirred at reflux for 2.5 h under nitrogen. The final reaction mixture was orange-red. After cooling to room temperature, 2 mL of 1.0 M HPF_6 (aq) were added to precipitate the product, which was isolated by filtration, washed with 0.1 M HPF_6 (aq) and ether, and dried under vacuum overnight. [$RuL_2(H_2L')](PF_6)_2$ was further purified by column chromatography using Sephadex DEAE A-25 as the column support and water as the eluent. The major band was collected and the eluent evaporated to a few mL using a rotary evaporator. HPF_6 (aq) (1 M, 0.4 mL) was then added to precipitate the [$RuL_2(H_2L')](PF_6)_2$. [$RuL_2(H_2L')](PF_6)_2$ was isolated by filtration, washed with 0.1 M HPF_6 (aq) and ether, and dried under vacuum overnight. Elemental analysis for $C_{32}H_{24}N_6O_4P_2F_{12}Ru \cdot 5H_2O$ gave (calculated values in parentheses) C, 37.31 (37.04); H, 3.13 (3.30); N, 8.10 (8.10). The chloride salt was isolated by taking the eluted band from the ion exchange column, adding a minimum amount of 1 M HCl (aq), and evaporating the solvent to dryness using a rotary evaporator. Elemental analysis for $C_{32}H_{24}N_6O_4Cl_2Ru \cdot 4H_2O$ gave (calculated values in parentheses) C, 47.77 (48.01); H, 3.92 (4.03); N, 10.41 (10.50).

$K_4[RuL'_3]$: Tetrapotassium tris(4,4′-dicarboxy-2,2′-bipyridyl)-ruthenate(II). $Ru(H_2L')_2Cl_2$[22] (0.215 g, 2.87×10^{-4} mol) was combined with H_2L' (0.0795 g, 3.26×10^{-4} mol), ca. 0.5 mL of triethylamine, 25 mL of water, and 25 mL of ethanol. The mixture was heated at reflux for 3.5 h and then cooled to room temperature. The ethanol was removed by rotary evaporation,

and ~ 0.5 g of NH_4PF_6 added to the solution. The mixture was then cooled to 5 °C. Precipitation of the crude product was induced by dropwise addition of 3 M HCl (aq) while stirring in an ice bath. The solid was collected on a fine-porosity glass frit and rinsed with acetone followed by diethyl ether. The crude product was then redissolved in 0.01 M $NaHCO_3$ (aq) and loaded onto an anion-exchange resin column (2.5 cm × 25 cm of Sephadex DEAE-A-25). Some impurities were eluted first using 0.2 M KI (aq) and discarded. The product was eluted using 0.4 M KI (aq), and the eluent was taken to dryness by rotary evaporation. The KI was removed by extraction with ethanol until some of the product dissolved in ethanol. The remaining KI was extracted with acetone, and the product isolated by filtration. Elemental analysis for $C_{36}H_{18}N_6O_{12}K_4Ru\cdot 6H_2O$ gave (calculated values in parentheses) C: 39.72 (39.59), N: 7.65 (7.70), H: 2.65 (2.77).

B. Methods. *1. Characterization of the Complexes.* The ^1H (500 MHz) NMR spectra were recorded on a Bruker AM 500 FT NMR spectrometer. Samples were prepared in D_2O with just enough NaOD added to dissolve the metal complex. The D_2O contained 1% DSS (3-(trimethylsilyl)-1-propanesulfonic acid, sodium salt) for reference (δ 0.00 ppm). All ^{15}N (50.70 MHz) and ^{13}C (125.77 MHz) spectra were recorded on a Bruker AMX-500 FT NMR spectrometer. These samples were either prepared in D_2O with NaOD added to dissolve the metal complex (with $K^{15}NO_3$ as the ^{15}N reference at 0.0 ppm and 1,4 dioxane as the ^{13}C reference at 66.5 ppm), or in d^6-DMSO (with $K^{15}NO_3$ as the ^{15}N reference at 0.0 ppm and d^6-DMSO used for the ^{13}C reference at 39.51 ppm).

Mass spectra were obtained with a ProSpecE FAB^+ mass spectrometer in low resolution mode or with an LCQ Electrospray mass spectrometer equipped with a quadrupole detector. Elemental analyses were performed by the Analytical Service at Caltech. Infrared spectra of KBr pellets of the sample were recorded on a Perkin-Elmer 1600 Series FTIR, normally with 2 cm^{-1} resolution. Electronic absorption spectra were recorded on a Hewlett-Packard 8452A diode array spectrophotometer. To obtain reproducible spectra, the solvent was buffered with 1.0 mM pyridine and 1.0 mM pyridinium triflate. The chloride salts of $Os(H_2L')_3^{2+}$, $RuL_2(H_2L')^{2+}$ and $OsL_2(H_2L')^{2+}$ were used because they are more soluble in methanol and ethanol. Emission spectra were recorded at room temperature using a PMT R406 (Products for Research, Inc.) photomultiplier tube cooled with dry ice. The solvent was methanol with 1.0 mM pyridine and 1.0 mM pyridinium triflate. The emission of $Os(H_2L')_2(NCS)_2$ was so weak that it could not be detected at room temperature. Instead, the emission spectrum of this complex was obtained by Prof. A. Maverick at Louisiana State University in an ethanol/methanol (4:1 v/v) glass at 77 K.

Ground state reduction potentials were determined using a standard three-electrode apparatus. The working electrode was a carbon disk electrode, the counter electrode was a Pt foil, and the reference electrode was a methanolic saturated calomel electrode (MSCE). The MSCE was periodically calibrated against an aqueous SCE (Fisher Scientific). Cyclic voltammograms were collected using either a Princeton Applied Research model 175 universal programmer and a Princeton Applied Research model 173 potentiostat/galvanostat or a BAS 100B electrochemical analyzer from Bioanalytical Systems. Differential pulse voltammetry (DPV) spectra were collected using a BAS 100B electrochemical analyzer. Methanol was used as the solvent because it was the only nonaqueous solvent into which 1 mM of most of the complexes could be dissolved. Except where noted, the supporting electrolyte was 1.00 M $LiClO_4$, and 10 mM pyridine and 10 mM pyridinium triflate were added to control the proton activity of the solution. For experiments with $Os(H_2L')_3^{2+}$ and $Ru(H_2L')_3^{2+}$, pyridine was omitted because its presence caused precipitation of the dye even at dye concentrations as low as 0.1 mM. Such a low concentration of the dye, coupled with the fact that the cyclic voltamogram occurred at very positive potentials where methanol is also oxidized, rendered the accurate determination of the oxidative electrochemical potential of $Ru(H_2L')_3^{2+}$ by cyclic voltammetry very difficult. The formal potentials of these complexes were therefore measured using DPV. In the case of $Ru(H_2L')_2(NCS)_2$, the cyclic voltammogram was irreversible in methanol. The electrochemical potential was therefore also measured using DPV. The redox behavior of $Ru(H_2L')_2(NCS)_2$ was more reversible in CH_3CN−1.00 M $LiClO_4$, and its cyclic voltammogram was obtained in this electrolyte. The pyridine/pyridinium triflate buffer was omitted in CH_3CN because it caused precipitation of the complex.

2. Preparation of Dye-coated Nanocrystalline TiO_2 Electrodes. The TiO_2 electrodes (Institut für Angewandte Photovoltaik) consisted of conducting glass (3 mm thick) coated with a transparent 5−6 μm thick layer of TiO_2 (measured by profilometry, Dektak 3030). The as-received electrodes were first treated by depositing a freshly made solution of 0.2 M $TiCl_4$ (aq) (from a 2.0 M $TiCl_4$ stock solution) overnight onto the TiO_2. The electrodes were then rinsed with water, rinsed with ethanol, dried with flowing nitrogen, and heated to 450 °C in air for 30 min. Once the electrodes were cooled to about 120 °C, they were immersed in an ethanolic solution containing 5 × 10^{-5} M to 1 × 10^{-4} M of the desired dye as well as 1.0 mM pyridine and 1.0 mM pyridinium triflate. Immersion was performed overnight to obtain high loadings, but was limited to only 15 min for experiments at low dye loadings. The absorbances of the ethanolic solutions containing a dye in a 1.0 cm path length were typically 0.7−1.3 at the maximum of the metal-to-ligand charge-transfer band of the complex. The $ML_2(H_2L')^{2+}$ complexes were isolated as the chloride salt and the PF_6^- salt; in this work, the PF_6^- salts of these complexes were used for adsorption onto TiO_2 because they yielded better open-circuit voltage values than the corresponding chloride salts. In the case of $M(II)L'_3{}^{4-}$ complexes, the potassium salts were utilized. In these potassium salts, the carboxylic groups are deprotonated and more pyridinium triflate was necessary to dissolve the dye in ethanol: the ethanolic solution contained 2.0 mM pyridinium triflate and 1.0 mM pyridine. The sources of the other complexes used for adsorption onto TiO_2 were the final purified materials described in the Experimental Section above. The UV−vis spectra of the electrodes were obtained prior to the photoelectrochemistry. The blank was a TiO_2 electrode that had been treated nominally identically to the other electrodes but that was immersed instead into an ethanolic solution that contained no dye.

3. *Photoelectrochemistry.* The current density−potential (J−E) curves and spectral response data were both recorded using a three-electrode potentiostatic setup with a Pt wire reference and Pt gauze counter electrode.[23] The distance between the working and counter electrodes was approximately 2 mm, and the solution was not stirred. The working electrode was illuminated through the conducting glass and the illuminated surface area was 0.25 cm^2. The cell was filled with electrolyte by using a syringe. The electrolyte consisted of 0.500 M LiI−0.040 M I_2/0.050 M pyridine−0.020 M pyridinium triflate in dry CH_3CN. Pyridine/pyridinium triflate were added to control the acidity of the electrolyte solution, thus stabilizing the

conduction band edge of the TiO_2 and hence the open-circuit photovoltage V_{oc}.[23] This particular buffer was chosen because the reagents are soluble in acetonitrile, and because the aqueous pK_a of pyridinium is 5.21 in water, which is near the point of zero charge for TiO_2 in aqueous solutions.[24−26] The electrolyte could be changed by refilling the cell with the new electrolyte without disassembling the cell. Refilling the cell by pushing through about 3 times the volume of the cell was found to be sufficient to replace the old electrolyte. This feature was utilized for the [LiI] study where electrolytes with different concentrations of LiI, I_2, and $LiClO_4$ were tested on the same electrode.

The presence of water was found to cause deterioration of the electrodes, so care was taken to reduce water levels as much as conveniently possible.[23] The electrolyte was kept in a dry Schlenk tube under nitrogen, and all cells were purged with nitrogen and then filled with the electrolyte. The cells were cleaned with absolute ethanol between measurements. These precautions led to greatly improved reproducibility. Once the electrodes were removed from the cell, they were observed to be visibly degraded outside the area that had been exposed to the electrolyte. For this reason, fresh electrodes were used in all experiments.

V_{oc} values between the Pt reference and working electrodes were recorded after 5 min of equilibration at open-circuit under the desired light intensity, or once the V_{oc} had reached a stable value. This equilibration time was especially necessary immediately after current had passed through the cell. The V_{oc} measured using this procedure was consistently larger by about 20 mV than the V_{oc} deduced from the *x*-intercept of a *J*−*E* scan, regardless of whether the scan rate was 20 mV s^{-1} or 0.5 mV s^{-1}. The V_{oc} values reported herein were reproducible and did not change significantly over the course of several hours.

J−*E* data were collected using a Solartron SI 1287 Electrochemical Interface that was controlled with Coreware v. 2.1a software. The scan rate was 20 mV s^{-1}. All potentials were recorded vs a Pt wire that was immersed into the solution. The cell potential for the electrolyte (0.500 M LiI−0.040 M I_2/0.050 M pyridine−0.020 M pyridinium triflate in dry CH_3CN) was +0.08 V vs aq SCE. The cell was illuminated by an ELH-type W-halogen bulb and light intensities were determined using a calibrated silicon photodiode (Solarex). A 385 nm cutoff filter was used during measurements (but not during the calibration with the photodiode) to avoid direct excitation of electron−hole pairs in the titanium dioxide. Prior to obtaining *J*−*E* data, the cell was maintained at short-circuit under illumination for 30 s because initial *J*−*E* scans showed higher currents, which dropped down rapidly and then leveled off to a constant, reproducible value, which was the one reported herein. The *J*−*E* properties of these junctions remained stable for several hours. When the pyridine/pyridinium triflate was not added to the electrolyte solution, however, the photocurrent was unstable and continually declined on every *J*−*E* scan from the short circuit potential to the open circuit potential.

Where indicated, *J*−*E* data were corrected for ohmic resistance and concentration overpotentials in the solution, using procedures that have been described in detail previously.[27,28] A platinum foil working electrode, placed in a nominally identical position as the various TiO_2 electrodes, was used to obtain the *J*−*E* data needed to perform these corrections. The ohmic resistance of the cell was determined to be 56 ohm. The contribution of η_{conc} was, in many cases, estimated to be negligible due to the relatively low currents that flowed in the cell relative to the mass-transfer-limited currents that were available in the system.

Spectral response data were obtained by biasing the cell to short circuit and measuring the current with a Keithley 177 microvolt DMM multimeter. Monochromatic light was obtained from a Spex 1682A tungsten lamp mated to a Spex 1681B monochromator equipped with 2.5 mm slits. The monochromator output beam was split with a glass slide into sample and reference beams. The system calibration was performed by placing a calibrated Si photodiode (obtained from United Detector Technology, Inc.) in the same position as the TiO_2 working electrode and measuring the photocurrent at short circuit from each system. The calibrated diode had a mask with the same surface area as the TiO_2 working electrode, and the ratio of the response of the TiO_2 cell to that of the calibration diode gave the quantum yield for the TiO_2 cell. Any variation in the light intensity between measurements was accounted for by dividing the current obtained from the sample or calibration device by the current produced by the reference beam, which was directed onto a separate, second silicon photodiode (also obtained from United Detector Technology, Inc.). The quantum yields were therefore computed using the following equation:

$$\Phi_{smp} = \Phi_{cal}\left(\frac{I_{smp}/\text{area}}{I_{ref,smp}}\right)\left(\frac{I_{ref,cal}}{I_{cal}/\text{area}}\right) \quad (1) \qquad (1)$$

where Φ_{smp} and Φ_{cal} are the quantum yields for the sample and the calibrated photodiode, respectively, I_{smp} and I_{cal} are the photocurrents obtained at the sample and at the calibrated diode, respectively, and I_{ref} is the photocurrent of the reference diode. The external quantum yields obtained using this measurement procedure were not corrected for optical scattering or reflection losses nor for incomplete absorption by the dye at certain wavelengths.

For the TiO_2 electrodes, the dark current was not negligible compared to the light current at the low light levels used in the spectral response experiments, and the dark current value also tended to drift slightly over time. The dark current was therefore measured periodically and the photocurrent was obtained by subtracting the dark current from the measured total current. At very low light intensity, i.e., at photocurrents less than approximately 2 μA cm^{-2}, the quantum yield was found to be dependent on the light intensity, so data reported herein always refer to measurements performed at current densities that are higher than this value.

III. Results

A. NMR Spectra of the Various Complexes. Nitrogen-15 and Carbon-13 NMR studies were carried out on the doubly labeled species $K^{15}N^{13}CS$, $RuL_2(^{15}N^{13}CS)_2$, $Ru(H_2L')_2(^{15}N^{13}CS)_2$ and $Os(H_2L')_2(^{15}N^{13}CS)_2$, in order to determine whether the NCS^- ligands were N- or S- bound to the ruthenium and osmium metal centers in complexes that contained the 2,2′-bipyridine-4,4′-dicarboxylic acid ligands.

1. ^{1}H NMR Characterization. The ^{1}H NMR spectral data for the complexes in D_2O/NaOD are listed in Table 1. In this solvent, the carboxylate groups on the ligands were deprotonated. The ^{1}H NMR spectra of ML'_2X_2,$^{4-}$ where X is Cl^-, NCS^-, or CN^-, all showed six signals in the aromatic region, arising from the six inequivalent protons on each of two equivalent 4,4′-dicarboxylic acid-2,2′-bipyridyl ligands. This splitting pattern is indicative of *cis*-ML'_2X_2 structures having C_2 symmetry. The assignments are based on integration, splitting patterns and chemical shifts. In the case of $RuL'_2(NCS)_2$,$^{4-}$ the

TABLE 1: ^{1}H NMR Data for the Complexes in D_2O/NaOD[a]

complex	chemical shift δ (ppm)	proton−proton coupling constants ^3J (Hz)	^4J (Hz)	assignment
		C_2 Complexes		
$RuL'_2(NCS)_2^{4-}$	9.46	d 6		a
	8.84	s		*c*
	8.68	s		d
	8.12	dd 6	2	b
	7.73	d 6		f
	7.43	dd 6	2	e
$RuL'_2(CN)_2^{4-}$	9.53	d 6		a or f
	8.79	s 1		c or d
	8.70	s		c or d
	7.99	dd 6	2	b or e
	7.69	d 6		a or f
	7.54	dd 6	2	b or e
$OsL'_2Cl_2^{4-}$	9.59	d 6		a or f
	8.84	s		c or d
	8.63	s		c or d
	7.94	dd 6	2	b or e
	7.61	d 6		a or f
	7.14	dd 6	2	b or e
$OsL'_2(NCS)_2^{4-}$	9.34	d 6		a or f
	8.82	s		c or d
	8.64	s		c or d
	7.98	dd 6	1	b or e
	7.63	d 6		a or f
	7.26	dd 6	1	b or e
$OsL'_2(CN)_2^{4-}$	9.64	d 6		a or f
	8.79	s		c or d
	8.70	s		c or d
	7.91	dd 6	2	b or e
	7.66	d 6		a or f
	7.49	dd 6	2	b or e
RuL_2L'	8.87 (rel I:1)	s	1	c
	8.54 (rel I:2)	two d 8		g and h
	8.05 (rel I:2)	two vt na	na	f and i
	7.92 (rel I:1)	d 6		a
	7.81 (rel I:1)	d 5		
	7.79 (rel I:1)	d 6		d and k
	7.66 (rel I:1)	dd 6	2	b
	7.37 (rel I:2)	two vt na	na	e and j
OsL_2L'	8.85 (rel I:1)	s		c
	8.51 (rel I:2)	two d ∼7		g and h
	8.86 (rel I:3)	m na	na	a, f and i
	7.12 (rel I:1)	d 5		d or k
	7.68 (rel I:1)	d 6		d or k
	7.55 (rel I:1)	dd 6	n.	b
	7.28 (rel I:2)	two vt n.a.	na.	e and j
		D_3 Complexes		
RuL'_3^{4-}	8.88	s		c
	7.88	d 6		a
	7.68	dd 6	2	b
OsL'_3^{4-}	8.86	s		c
	7.78	d 6		a
	7.58	dd 6	2	b

[a] All NMR spectra were recorded in D_2O with added NaOD. All chemical shifts were reported as referenced to DSS as an internal standard (0.00 ppm). na = not assigned, s = singlet, d = doublet, dd = doublet of doublets, vt = virtual triplet, m = multiplet, rel I = relative integration.

signals were further assigned based on literature values.[29,30] The chemical shifts for $RuL'_2(NCS)_2^{4-}$ reported here agree with those previously reported.[29,31] The ^{1}H NMR spectra of $RuL'_2(NCS)_2^{4-}$ and $OsL'_2(NCS)_2^{4-}$ also showed a series of much smaller signals that we ascribe to the mixed-bound $ML'_2(NCS)(SCN)^{4-}$ complexes. Most of those signals overlapped with the more intense signals arising from the all-nitrogen bound complex, except for the most downfield doublet. This doublet is associated with hydrogen (a) of one of the L′ ligands, and appeared at 9.64 ppm for $RuL'_2(NCS)_2^{4-}$ and 9.54 ppm for $OsL'_2(NCS)_2$.$^{4-}$ The ratio of the major product to the mixed-bound product was about 7:1. This ratio could not be increased upon increasing the reaction time. The presence of the mixed-bound complex of ruthenium was also observed by Grätzel and co-workers.[31]

The ^{1}H NMR spectra for the ML_2L' complexes illustrate that these complexes possess C_2 symmetry, having two equivalent 2,2-bipyridine ligands (L) each with eight inequivalent protons, and one 4,4′-dicarboxylato-2,2′-bipyridyl ligand (L′) possessing an axis of symmetry that produces three sets of two equivalent protons. Eleven inequivalent protons in each complex give rise to the resonances (with some overlapping of the signals). The aromatic region of the ^{1}H NMR spectra of ML'_3^{4-} complexes showed a simple ^{1}H NMR spectrum that consisted of one singlet and two doublets, indicative of D_3 symmetry.

2. ^{15}N and ^{13}C NMR Study to Determine Linkage Isomerism in NCS$^-$ Complexes. Two previous studies (one examining ^{14}N and the other utilizing ^{15}N NMR) on a variety of metal complexes have shown that S-bound metal thiocyanato complexes (M−S−C≡N) have a nitrogen chemical shift slightly downfield of that observed for the free thiocyanate ion (represented as KSCN or NaSCN dissolved in the NMR solvent of choice) whereas nitrogen-bound metal isothiocyanato complexes (M−N≡C−S) exhibit ^{14}N or ^{15}N resonances "shifted by a comparatively large amount upfield of the free thiocyanate ion".[32,33] The nitrogen chemical shifts of metal thiocyanato and isothiocyanato complexes reported in these two studies are compiled in Table 2. In this tabulation, all chemical shifts have been either measured or calculated as referenced to the KNO_3 standard at 0.0 ppm. Additionally, we have chosen the convention of reporting signals that occur upfield of KNO_3 as having negative chemical shifts and those that occur downfield from KNO_3 as having positive chemical shifts.

^{15}N NMR data for doubly labelled complexes and for free doubly labelled thiocyanate obtained in this work are reported in Table 3. In all spectra, one principal doublet was observed, representing a ^{15}N signal split by a single adjacent ^{13}C atom in the nitrogen NMR spectrum. The ^{15}N resonances observed for $RuL'_2(^{15}N^{13}CS)_2^{4-}$ and $OsL'_2(^{15}N^{13}CS)_2^{4-}$ in D_2O/NaOD are shifted by significantly large amounts upfield of the free thiocyanato ion, suggesting that both $RuL'_2(NCS)_2^{4-}$ and $OsL'_2(NCS)_2^{4-}$ are isothiocyanato complexes bound to the metal through nitrogen. In support of this assignment, the noncarboxylated analogue of $Ru(H_2L')_2(NCS)_2$, $RuL_2(NCS)_2$, which has been established by X-ray crystallography to have nitrogen-bound thiocyanato ligands,[34] has a very similar chemical shift for the labeled $^{15}N^{13}CS^-$ isothiocyanato ligand (−241.8 for $RuL_2(^{15}N^{13}CS)_2$ vs −245.2 ppm for $RuL'_2(^{15}N^{13}CS)_2$).$^{4-}$ A crystallographic structure of the ethyl ester derivative of $Ru(H_2L')_2(NCS)_2$, Ru(4,4′-$(COOEt)_2$-2,2′-bipyridine)$_2$$(NCS)_2$, shows that this analogue also has N-bound isothiocyanato ligands.[29]

Previously, it was reported that the chemical shift in the ^{13}C NMR spectrum of metal thiocyanate complexes could be used as a diagnostic tool to determine the linkage isomerism of the NCS^- ligand.[35] Kargol et al. analyzed a series of S-bound and N-bound thiocyanate compounds and observed upfield chemical shift differences ranging from 3−20 ppm relative to ionic thiocyanate for the ^{13}C shift of S-bound complexes and downfield chemical shift differences of 1−16 ppm for the ^{13}C signal of N-bound complexes. These data were generalized into the simple rule that S-bound thiocyanate shows chemical shifts upfield relative to the ionic thiocyanate and N-bound NCS^- shows downfield chemical shifts relative to the ionic thiocyanate. There were a few exceptions to this rule, however, in which the ^{13}C resonance of N-bound isothiocyanato ligands appeared

TABLE 2: A Comparative Study of δ ^{15}N Chemical Shift for M−SCN and M−NCS Complexes

compound	solvent	δ ^{15}N (NO_3^- = 0.0 ppm)	δ ^{14}N (NO_3^- = 0.0 ppm)	ref
KSCN	H_2O		−166	32
KSCN	CH_2Cl_2[a]	−160.2		33
KSCN	D_2O	−170.8		this work
KSCN	d^6-DMSO	−156.0		this work
C_2H_5SCN	$CHCl_3$		−98.5	32
C_2H_5NCS	pure		−268	32
M−SCN complexes				
$Na_2[Pd(SCN)_4]$	H_2O		−148	32
$Na_2[Pt(SCN)_4]$	H_2O		−166	32
$Na_2[Rh(SCN)_6]$	H_2O		−158	32
$Na_2[Ir(SCN)_6]$	H_2O		−163	32
$Na_2[Hg(SCN)_4]$	H_2O		−157	32
$(Bu_4N)_2[Pd(SC^{15}N)_4]$	CH_2Cl_2[a]	−123.9[b]		33
$(Bu_4N)_2[Pd(SC^{15}N)_4]$[c]	CH_2Cl_2	−125.1[b]		33
$(Bu_4N)_2[Hg(SC_{15}N)_4]$	CH_2Cl_2[a]	−134.7[b]		33
M−NCS Complexes				
cis-$[Pt(NCS)_2(Bu_3P)_2]$	$CHCl_3$		−302	32
cis-$[Pt(NCS)_2(Bu_2PhP)_2]$	$CHCl_3$		−249	32
trans-$[PtH(NCS)(Et_3P)_2]$	$CHCl_3$		−239	32
cis-$[Pt(NCS)_2(Bu_3As)_2]$	$CHCl_3$		−303	32
trans-$[Ni(NCS)_2(Et_3P)_2]$	$CHCl_3$		−293	32
trans-$[Ni(NCS)_2(Bu_2PhP)_2]$	$CHCl_3$		−291	32
$Na_2[Cd(NCS)_4]$	H_2O		−178	32
$Na_2[Cd(NCS)_4]$	CH_3OH		−220	32
$Na_2[Zn(NCS)_4]$	CH_3CH_2OH		−255.5	32
$(Bu_4N)_2[Zn(^{15}NCS)_4]$	CH_2Cl_2[a]	−218.1[b]		33
$(Bu_4N)_2[Cd(^{15}NCS)_4]$	CH_2Cl_2[a]	−200.5[b]		33
trans-$[Pt(^{15}NCS)_2(n-Bu_3P)_2]$[d]	CH_2Cl_2[a]	−306.0[b]		33
$Mg(H_2O)_x(NCS)_y(OH)_z$	H_2O	−193 to −197[e]		40
$K_2[Ru(NCS)_5(NO)]$	H_2O		−268	32

[a] Solvent may be CH_2Cl_2, although the solvent was not explicitly stated for each sample. [b] Value of δ reported here as referenced to NO_3^- at 0.0 ppm: values were originally reported with a reference of NH_4Cl = 0 ppm. On a relative scale, NO_3^- appears at 376.53 ppm and NH_4Cl appears at 27.34 ppm.[33,41] [c] Thiocyanate ligand was determined to be bound through sulfur from the analysis of the ^{195}Pt chemical shift and the observed $^3J(^{195}Pt-^{15}N)$ coupling constant of 12 Hz. [d] Thiocyanate ligand was determined to be bound through nitrogen from the analysis of the ^{195}Pt chemical shift and the observed $^1J(^{195}Pt-^{15}N)$ coupling constant of 589 Hz. [e] In this study, ^{15}N chemical shifts were reported as $\Delta\delta$ relative to $KSC^{15}N$. Values reported here have been readjusted relative to NO_3^- at 0.0 ppm.

TABLE 3: ^{13}C and ^{15}N NMR Data

compound	NMR solvent	δ ^{13}C	$^1J^{13}C$-^{15}N (^{13}C NMR)	δ ^{15}N	^1J $^{13}C-^{15}N$ (^{15}N NMR)	ref
$KS^{13}C^{15}N$	D_2O/NaOD	132.9[a]	13.56 Hz	−170.8[c]	13.56 Hz	this work
$RuL'_2(^{15}N^{13}CS)_2^{4-}$	D_2O/NaOD	132.0[a]	28.8 Hz	−234.3[c]	27.1 Hz	this work
$OsL'_2(^{15}N^{13}CS)_2^{4-}$	D_2O/NaOD	126.4[a]	32.2 Hz	−258.6[c]	33.9 Hz	this work
Ionic $S^{13}CN^-$	D_2O/NaOD	134.2				31
$RuL'_2(N^{13}CS)_2^{4-}$	D_2O/NaOD	132.8				31
$RuL'_2(N^{13}CS)\ (S^{13}CN)^{4-}$	D_2O/NaOD	132.8, 126.8				31
$KS^{13}C^{15}N$	d^6-DMSO	129.6[b]	10.17 Hz	−158.6[c]	13.56 Hz	this work
$Ru(H_2L')_2(^{15}N^{13}CS)_2$	d^6-DMSO	134.6[b]	28.8 Hz	−245.2[c]	27.2 Hz	this work
$RuL_2(^{15}N^{13}CS)_2$	d^6-DMSO	133.4[b]	28.8 Hz	−241.8[c]	27.1 Hz	this work
Ionic $S^{13}CN^-$	d^4-MeOH	133.6				31
$Ru(H_2L')_2(N^{13}CS)_2$	d^4-MeOH	135.4				31
$Ru(H_2L')_2(N^{13}CS)\ (S^{13}CN)$	d^4-MeOH	136.0, 124.2				31
$Ru(H_2L')_2(S^{13}CN)X$ ($X = S^{13}CN^-, Cl^-$)	d^4-MeOH	124, 125				31

[a] δ ^{13}C shifts referenced to dioxane at 66.5 ppm. [b] δ ^{13}C shifts referenced to DMSO at 39.51 ppm. [c] δ ^{15}N shifts referenced to KNO_3 at 0.0 ppm.

slightly (approximately 1 ppm) upfield of that reported for ionic thiocyanate in the same solvent.

The ^{13}C NMR data for our doubly labeled complexes are reported in Table 3, along with the ^{13}C NMR data reported by Grätzel and co-workers on $RuL'_2(N^{13}CS)_2^{4-}$ and $RuL'_2(N^{13}CS)(S^{13}CN)^{4-}$ in both D_2O/NaOD and in d^4-methanol (presumably being the fully protonated species under these conditions) for comparison. In all but one case (for the sample of $RuL'_2(^{15}N^{13}CS)_2^{4-}$) only one doublet was detected in each spectrum, which indicated that the syntheses produced only one product, to the detection limit of the NMR method. In the ^{13}C NMR spectrum of $RuL'_2(^{15}N^{13}CS)_2^{4-}$ however, another signal was observed at the 10% level, which likely arises from the presence of a mixed-bound ligand species that is similar to the species reported by Grätzel and co-workers.[31]

The ^{13}C NMR signals of $RuL'_2(^{15}N^{13}CS)_2^{4-}$ and $OsL'_2(^{15}N^{13}CS)_2^{4-}$ measured in D_2O/NaOD exhibit ^{13}C chemical shifts upfield of free thiocyanate ion by 0.9 and 6.5 ppm respectively (Table 3). Applying the general rule discussed above would suggest that the thiocyanates are bound through the sulfur atom, which is inconsistent with all the other NMR data reported in this work. Grätzel and co-workers also observe the ^{13}C chemical shifts for $RuL'_2(N^{13}CS)_2^{4-}$ in both D_2O/NaOD and d^4-methanol to appear upfield of the free thiocyanate ion in the same solvent.[31] However, they also observed another lower intensity peak further upfield, so they assigned the principle product of the reaction between the cis-$Ru(H_2L')_2Cl_2$ starting material and the thiocyanate ligand to produce an N-bound isothiocyanate species. Unless a resonance is observed further upfield that could be attributed to S-bound thiocyanate, we cannot unequivocally

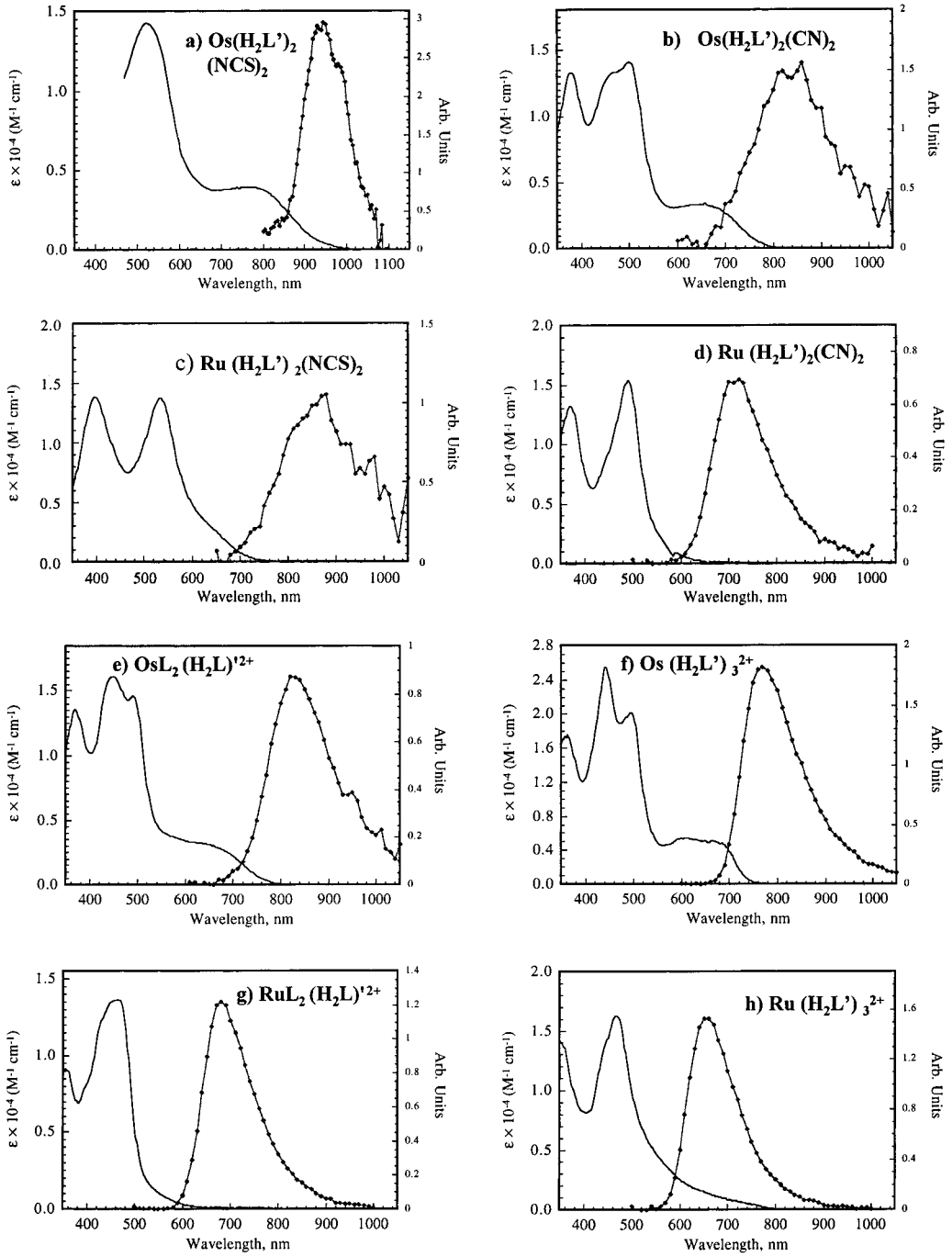

Figure 1. UV−vis absorption spectra (solid line, no circle) and emission spectra (circle) of the complexes in methanol containing 1.0 mM pyridine and 1.0 mM pyridinium triflate.

assign the isomer linkage of thiocyanate using ^{13}C NMR in D_2O/NaOD. Two low intensity doublets at 133.75 and 121.55 ppm were observed in the ^{13}C NMR spectrum of $RuL'_2(^{15}N^{13}CS)_2$,$^{4-}$ possibly arising from a species with mixed-linkage NCS^- ligands $RuL'_2(^{15}N^{13}CS)(S^{13}C^{15}N)^{4-}$ similar to those reported by Grätzel and co-workers.[31]

The ^{13}C NMR spectra of the $RuL_2(^{15}N^{13}CS)_2$ and $Ru(H_2L')_2(^{15}N^{13}CS)_2$ complexes in d^6-DMSO showed downfield ^{13}C shifts relative to ionic thiocyanate of 3.8 and 5.0 ppm respectively (Table 3), indicative of linkage through the nitrogen. Both $Ru(H_2L')_2(NCS)_2$ and its non-carboxylated analogue showed similar ^{15}N and ^{13}C chemical shifts, confirming the above assignment that the linkage occurs through the nitrogen.

B. Absorption, Emission, and Electrochemical Properties of the Os and Ru Complexes. Figure 1 presents the electronic absorption and emission spectra of the Os and Ru complexes used in this work. The protonation states of the L′ ligands are not completely known in the presence of pyridine and pyridinium in these nonaqueous solvents, but for consistency in discussions of the spectral and electrochemical properties of these species, the complexes are referred to below using their fully protonated formulations. For a given ligand environment, the Os complexes all showed an additional absorption band at longer wavelengths than the Ru complexes. This lower energy band had a smaller extinction coefficient than that of the main metal-to-ligand charge transfer (MLCT) bands (Table 4). The red shift in the absorption of the Os complexes relative to the analogous Ru complexes is consistent with expectations of an enhanced oscillator strength for an electronic transition between the ground state and the triplet excited state of the Os

TABLE 4: Spectrochemical and Electrochemical Properties of the Complexes

complex	abs max/nm (ϵ/10^4 M^{-1} cm^{-1})[a]			emission[b]	$E^{\circ\prime}$, V vs aq SCE[d]	estimated E_{0-0} (eV)	estimated $E^{\circ\prime *}$ (V vs SCE)
$Os(H_2L')_2(NCS)_2$	412 (1.43 ± 0.05)	530 (1.51 ± 0.06)	~ 780 (0.5)	940[c]	0.42	1.4	−1.0
$Ru(H_2L')_2(NCS)_2$	398 (1.24 ± 0.03)	538 (1.21 ± 0.03)		880	0.68[e], 0.80[f]	1.8	−1.1
$Os(H_2L')_2(CN)_2$	382 (1.40 ± 0.05)	508 (1.44 ± 0.05)	~ 680 (0.368 ± 0.005)	840	0.72	1.8	−1.1
$Ru(H_2L')_2(CN)_2$	376 (1.31 ± 0.01)	496 (1.49 ± 0.01)		720	1.08[g]	2.0	−0.9
$OsL_2(H_2L')^{2+}$	448 (1.68 ± 0.05)	494 (1.48 ± 0.05)	~ 640 (0.4)	820	0.81	1.7	−0.9
$RuL_2(H_2L')^{2+}$	356 (1.01 ± 0.06)	470 (1.39 ± 0.04)		680	1.23	2.1	−0.9
$Os(H_2L')_3^{2+}$	442 (2.48 ± 0.02)	496 (2.02 ± 0.02)	~ 640 (0.6)	770	1.01[h]	1.8	−0.8
$Ru(H_2L')_3^{2+}$		464 (1.99 ± 0.08)		660	1.40[h,i]	2.1	−0.7

[a] In EtOH with 1 mM pyridine and 1 mM pyridinium triflate; ϵ are averages of 3 or more solutions. [b] At room temperature in MeOH with 1 mM pyridine and 1 mM pyridinium triflate [c] In EtOH/MeOH 4:1 glass at 77 K. [d] In MeOH with 10 mM pyridine, 10 mM pyridinium triflate and 1.0 M $LiClO_4$; determined by cyclic voltammetry. [e] Irreversible; determined by DPV. [f] In acetonitrile with 1.0 M $LiClO_4$; determined by cyclic voltammetry; reversible. [g] Quasireversible. [h] In MeOH with 10 mM pyridinium triflate and 1.0 M $LiClO_4$. [i] Determined by DPV.

complexes.[11] In addition, this lowest MLCT band is red-shifted when the ligands are changed from L (or H_2L') to CN^- to NCS^-, consistent with an increase in electron density on the metal resulting in destabilization of the metal t_{2g} orbitals. As expected, the emission spectra for the Os complexes were also red-shifted relative to those of the Ru complexes having identical ligands.

Table 4 also displays the ground state formal reduction potentials of these various complexes. All the osmium complexes displayed reversible cyclic voltammograms, whereas $Ru(H_2L')_2(NCS)_2$ displayed irreversible behavior in methanol. Consequently, the electrochemistry of the Ru complex was determined by DPV. $Ru(H_2L')_2(NCS)_2$ displayed more reversible behavior in CH_3CN, and its formal potential determined in CH_3CN, $E^{\circ\prime} = 0.80$ V vs SCE, is in good agreement with the reported value of $E^{\circ\prime} = 0.85$ vs SCE.[4] The difference between our measurement and the reported value could be due to a difference in the dye protonation state during the measurements. The formal potential of these dyes was observed in our work to be pH-dependent, as would be expected of acidic redox species.[36] For instance, the formal potential of $K_4[RuL'_3]$ was 1.25 V vs SCE in methanol with no pyridine or pyridinium present, but was 1.4 V vs SCE in the presence of 10 mM pyridinium. Also, the value of the formal potential of $Os(H_2L')_2(NCS)_2$ decreased upon addition of higher concentrations of pyridine. These results suggest that deprotonation lowers the value of $E^{\circ\prime}$, which is consistent with the expectation that more electron-rich ligands will render the metal center easier to oxidize and therefore yield a more negative $E^{\circ\prime}$ value.

As expected, the redox potentials of the Os complexes were more negative than those of the analogous ruthenium complexes. Also, within a series with the same metal, the trend for the ground-state redox potential $E^{\circ\prime}$[M(III)/M(II)] was

$$M(H_2L')_2(NCS)_2 < M(H_2L')_2(CN)_2 < ML_2(H_2L')^{2+} < M(H_2L')_3^{2+}$$

where M is Os or Ru. This trend correlates with the electron donating/π-accepting properties of the ligands around the metal center. Ligands with more electron donating properties (such as NCS^-) will confer additional stability on the M(III) oxidation state relative to the M(II) oxidation state, which will produce a more negative ground-state M(III)/M(II) redox potential. Increasing the π-acceptor properties of the ligands, however, leads to stabilization of the metal t_{2g} symmetry d-orbitals, which therefore produces a more positive M(III)/M(II) formal potential if all other factors are held constant. The ground state redox potentials can therefore be readily fine-tuned by varying the metal and the ligands in this series of complexes.

The excited-state redox potentials, $E^{\circ\prime}$[M(III)/M(II)]*, were estimated using eq 2:

$$E^{\circ\prime *} = E^{\circ\prime} - \mathbf{E}_{0-0}/q \qquad (2)$$

where $E^{\circ\prime}$ is the formal reduction potential of the ground state, $E^{\circ\prime *}$ is the formal reduction potential of the excited state (for the half-reaction M(III) + e^- → M(II)*), and $\mathbf{E}_{0-0}$ is the minimum energy between the ground state and excited state. $\mathbf{E}_{0-0}$ was estimated as the intersection between the absorption and emission spectra of the dye of concern (Figure 1, Table 4). The $E^{\circ\prime *}$ values for the osmium complexes were similar to those for the corresponding ruthenium complexes. This is expected because the electron density in the MLCT excited state of these sytems is centered primarily on the bipyridyl ligands. The π^* orbitals of the carboxylated bipyridyl ligand lie at lower energy than those of the noncarboxylated bipyridyl. As a result, the excited-state potential of the $M(H_2L')_3^{2+}$ complex is more positive than that of the $ML_2(H_2L')^{2+}$ complex. The lower apparent $E^{\circ\prime *}$ values for the $M(H_2L')_3^{2+}$ complexes could also arise because their ground-state redox potentials were measured at a different pH than the other complexes; also the pK_a values for the ligands in the excited state of the complex may be different than the pK_a values for the ligands in the ground state of the complex. Further trends among the $E^{\circ\prime *}$ values are not considered to be significant due to the error associated with the determination of these excited-state potentials.

C. Spectral Response Characteristics of Os- and Ru-Coated TiO_2 Electrodes. Figure 2 displays the spectral response characteristics, collected under short-circuit conditions, of the various dye-coated TiO_2 electrode systems studied in this work. As expected, the spectral response of each dye-coated TiO_2 electrode shows a strong correlation with the absorption spectrum of the metal complex.

Sensitization with $Ru(H_2L')_2(CN)_2$ produced very high maximum external quantum yields, with the analogous $Os(H_2L')_2$-

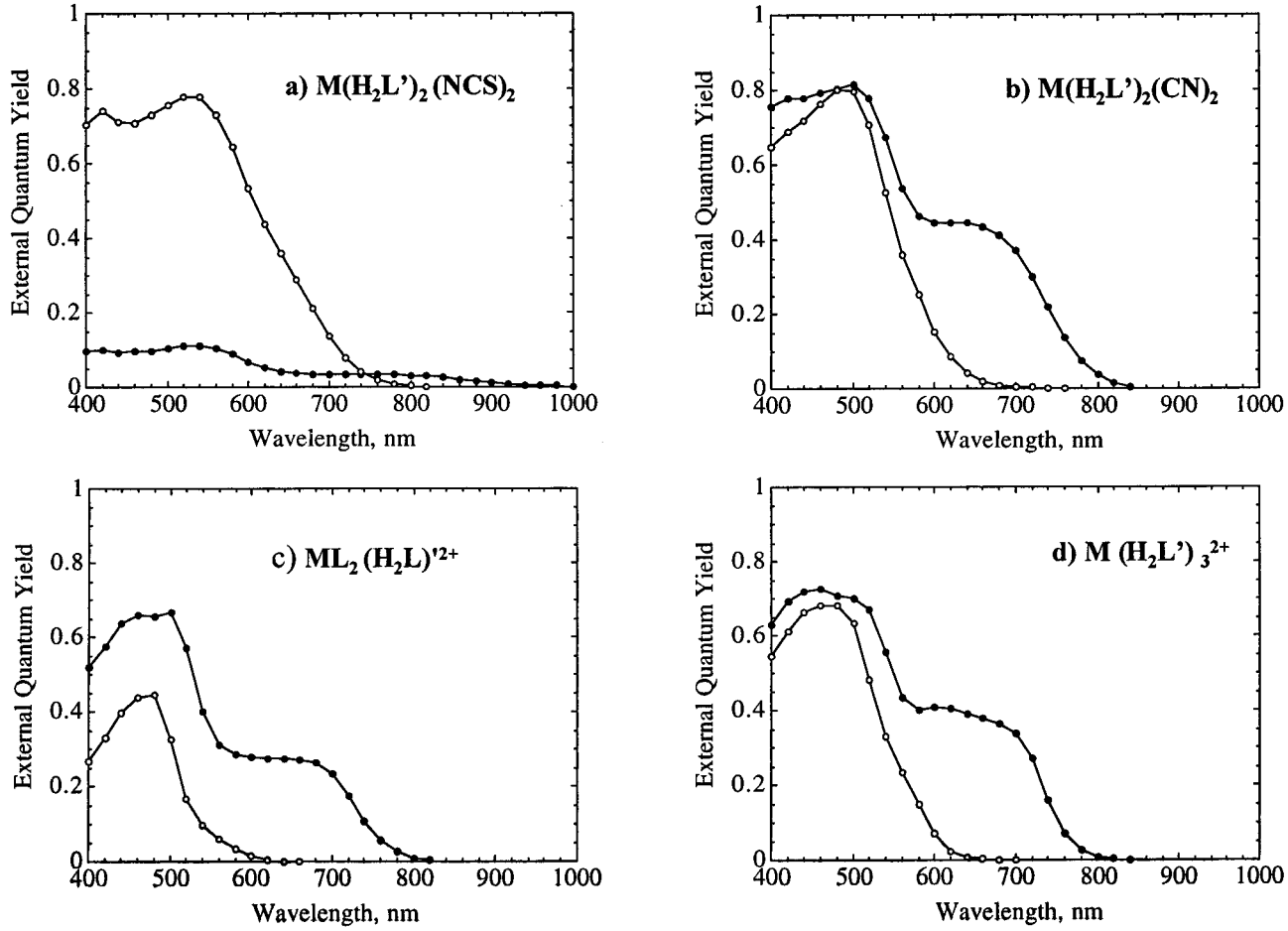

Figure 2. Spectral response data for the dye-coated TiO_2 electrodes. Each curve represents the average of three or more measurements. The filled circles represent the osmium complexes and the open circles are data for the ruthenium complexes. (a) $M(H_2L')_2(NCS)_2$, (b) $M(H_2L')_2(CN)_2$, (c) $ML_2(H_2L')^{2+}$, (d) $M(H_2L')_3^{2+}$, where *M* is the metal center.

$(CN)_2$ complex yielding similar maximum quantum yields and even better response in the red region of the spectrum. The $Ru(H_2L')_3^{2+}$ and $Os(H_2L')_3^{2+}$ complexes showed quantum yields similar to each other, with the Os complex again showing an improved response in the red relative to the Ru system. Similar enhancements in the red response were also observed in a comparison between the $RuL_2(H_2L')^{2+}$ and $OsL_2(H_2L')^{2+}$ systems. In contrast, although the red response was improved by changing from $Ru(H_2L')_2(NCS)_2$ to $Os(H_2L')_2(NCS)_2$, the Os complex yielded very low ($\Phi \approx 0.1$) steady-state quantum yields throughout the visible region. This phenomenon was investigated in detail and is discussed below. Even the complexes with the most positive excited-state redox potentials, the $Os(H_2L')^{2+}$ and $Ru(H_2L')^{2+}$ systems, produced high maximum quantum yields for injection. On an overall basis, the $Os(H_2L')_2(CN)_2$-, $Ru(H_2L')_2(NCS)_2$-, and $Os(H_2L')_3^{2+}$-coated electrodes had the spectral responses that were best matched for illumination by sunlight.

The maximum external quantum yield for a typical electrode containing each dye was corrected for the absorbance of the dye using eq 3:

$$\Phi_{\text{corrected}} = \frac{\Phi_{\text{external}}}{\left(\frac{100 - \%T}{100}\right)} \quad (3)$$

where $\%T$ is the percent transmittance of the dye-coated electrode at the wavelength of maximum external quantum yield. The corrected quantum yields are reported in Table 5. Note that the relatively low external quantum yield of $RuL_2(H_2L')^{2+}$ is due to the incomplete absorption of the light by the dye-coated electrode at this loading level. When the external quantum yield is corrected for the incomplete absorption of the dye, the quantum yield is 0.9. The corrected quantum yields approached unity for all the dyes except $Os(H_2L')_2(NCS)_2$, which only displayed a value of $\Phi = 0.12$.

TABLE 5: External and Corrected Quantum Yields (QY) for a Representative Dye-Coated Electrode

complex	max external QY	abs for electrode at λ of max QY	% T	corrected QY
$Os(H_2L')_2(NCS)_2$	0.11	1.32	4.8	0.12
$Ru(H_2L')_2(NCS)_2$	0.80	1.13	7.4	0.86
$Os(H_2L')_2(CN)_2$	0.81	0.83	14.8	0.95
$Ru(H_2L')_2(CN)_2$	0.83	1.08	8.3	0.91
$OsL_2(H_2L')^{2+}$	0.65	0.50	31.6	0.95
$RuL_2(H_2L')^{2+}$	0.43	0.28	52	0.90
$Os(H_2L')_3^{2+}$	0.71	1.26	5.5	0.75
$Ru(H_2L')_3^{2+}$	0.67	1.36	4.4	0.70

D. Current−Potential Behavior of Os- and Ru-Coated TiO_2 Electrodes. Figure 3 shows the *J*−*E* data, obtained both in the dark and under Air Mass (AM) 1.0 simulated illumination, for representative samples of the dye-coated TiO_2 electrodes that were studied in this work. The average short-circuit photocurrent density (J_{sc}) and open-circuit voltage (V_{oc}) values for each dye over a series of runs are reported in Table 6. Table 6 also reports the fill factors for the series-resistance-corrected *J*−*E* curves for the representative samples shown in Figure 3.

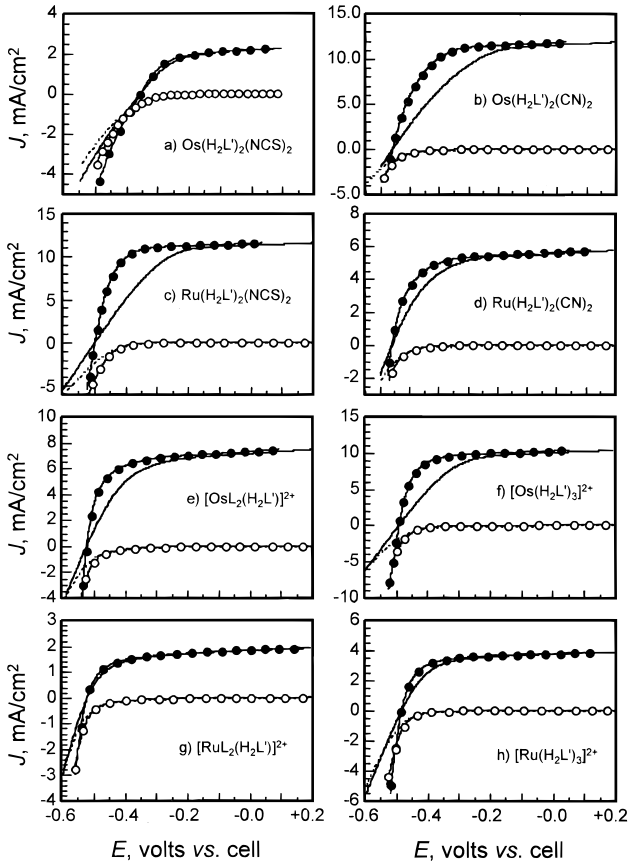

Figure 3. Current density vs potential behavior for representative TiO_2 electrodes sensitized with each dye. Filled circles are for illumination at 1 Sun, correced for cell resistance, while solid lines are uncorrected for cell resistance. Open circles show the dark response orrected for cell resistance, while dashed lines show the dark response uncorrected for cell resistance.

Figure 4 shows the series-resistance-corrected $J-E$ behavior for all of the dye-coated TiO_2 electrodes in the dark (Figure 4b) and at a light intensity sufficient to produce $J_{sc} = 1$ mA cm^{-2} (Figure 4a). The dark curves were different for the electrodes that had been coated with different metal complexes; similarly, at any specific potential in forward bias, the cathodic currents were different for each different electrode system. As a consequence, V_{oc} was different for every type of dye-coated electrode even when nominally identical short-circuit photocurrent densities, and thus nominally identical injected carrier densities, were obtained (Table 6).

The results described above were obtained at high dye loading levels, for which the TiO_2 electrodes were immersed into dye solutions at least 24 h before use. When TiO_2 electrodes were left in the dye solution for only 15 min, the current−potential curves for each of these types of electrodes were very similar, and so were the V_{oc} values at constant J_{sc} (Figure 5, Table 7). This behavior is expected for a situation in which the dark current is determined primarily by reduction of I_2 by electrons in the TiO_2, and when the rate of this process is not altered by the presence of adsorbed dye on the TiO_2 electrode surface. As expected, electrodes that had been immersed in the dye solution for only 15 min were much lighter in color than those immersed overnight in these dye solutions. Quantitative measurements of the absorbance of the electrodes (Table 7) confirmed this observation. Also reported in Table 7 are the photoelectrochemical properties obtained under ELH-type AM 1.0 illumination for the TiO_2 electrodes having low dye-loading levels. The short-circuit current densities displayed by these electrodes are still high, being 1.8−8 times lower than those observed for electrodes having a high dye loading level.

To understand why the $Os(H_2L')_2(NCS)_2$-coated electrodes showed such low currents and maximum quantum yield values, the photoelectrochemical properties of $Os(H_2L')_2(NCS)_2$-, $Ru(H_2L')_2(NCS)_2$-, and $RuL_2(H_2L')^{2+}$-coated electrodes were investigated at various I^- concentrations. When the added LiI and I_2 concentrations were doubled, the J_{sc} value at AM 1.0 illumination increased significantly in the case of $OsL'_2(NCS)_2$-coated electrodes but not in the case of $Ru(H_2L')_2(NCS)_2$- or $RuL_2(H_2L')^{2+}$-coated electrodes (see Table 8 and Figure 6). To ascertain whether the effect was due to increases in $[I^-]$ or $[Li^+]$, $J-E$ data were also collected in 0.5 M LiI/0.5 M $LiClO_4$/0.04 M I_2 (Figure 6a), but J_{sc} did not change significantly under these conditions relative to its value in the base electrolyte. The photocurrent for $Os(H_2L')_2(NCS)_2$-coated electrodes increased from 2.2 to 5.2 mA cm^{-2} upon increasing the iodide concentration 5-fold to a level of 2.5 M LiI/0.04 M I_2, which was the maximum concentration that could be obtained in this solvent. The maximum external quantum yield also increased from 0.1 to 0.2 at this level of I^-. The photocurrent and the maximum external quantum yield for the $Ru(H_2L')_2(NCS)_2$-coated TiO_2 electrodes did not increase significantly under similar conditions (Figure 7).

IV. Discussion

A. Purification and Characterization of the Complexes. Most of the syntheses were based on established methods, and the ^1H NMR spectra were readily assigned. We repeatedly observed during the course of this study that very pure dyes and control of proton activity during the adsorption process and the electrochemical measurements are apparently required to obtain good photoelectrochemical behavior from the sensitized electrodes. The best purification technique identified herein is anion exchange column chromatography, which not only separates complexes on the basis on their differing structures but also on the basis of their differing charges. Unfortunately, the $M(H_2L')_2(NCS)_2$ complexes could not be purified by ion-exchange column chromatography because these complexes sorbed strongly to the column support and did not elute even at very high electrolyte concentrations. These complexes were instead purified using size exclusion chromatography in methanol. Finally, the NCS^- linkage isomers could not be separated. One must therefore keep in mind that the $M(H_2L')_2(NCS)_2$ complexes might not be as pure as the other materials, and therefore may show lower open-circuit voltages and short-circuit currents than are possible for these systems.

The linkage isomerism of the NCS^- complexes was assigned based on our ^{15}N and ^{13}C NMR study. The $Ru(H_2L')_2(NCS)_2$ complex was assigned to contain predominantly nitrogen-bound isothiocyanato ligands. This assignment is in agreement with the prior literature for various ruthenium isothiocyanato complexes.[7,29,31,34,37,38] We believe that $Os(H_2L')_2(NCS)_2$ is predominantly an isothiocyanato complex based on the ^{15}N NMR data, as opposed to the more questionable interpretation of ^{13}C NMR data. Furthermore, these data indicate that ^{15}N NMR appears to be a more reliable spectroscopic tool than ^{13}C NMR spectroscopy for the assignment of linkage isomerism in metal complexes of the thiocyanate ligand.

B. Spectral Response Properties of Os- vs Ru-Coated TiO_2 Electrodes. An interesting question raised by the systems studied herein is whether the Os complexes, which have excited-state redox potentials that are similar to those of the analogous

TABLE 6: Photoelectrochemical Data

complex	N^a	V_{oc} ELH bulb, AM 1.0 (mV)	J_{sc} ELH bulb, AM 1.0 (mA cm^{-2})	ff[b] AM 1.0	max external QY	predicted J_{sc} ELH bulb 100 mW cm^{-2} (mA cm^{-2})[c]	predicted J_{sc} AM1.5 sun spectrum 100 mW cm^{-2} (mA cm^{-2})	V_{oc} 1.0 mA cm^{-2} (mV)
$Os(H_2L')'_2(NCS)_2$	3	360 ± 5	2.1 ± 0.3	0.55	0.11 ± 0.01	1.7	1.8	336 ± 6
$Ru(H_2L')_2(NCS)_2$	5	522 ± 6	10.8 ± 0.5	0.69	0.78 ± 0.03	10.8	10.4	432 ± 8
$Os(H_2L')_2(CN)_2$	4	569 ± 6	11.6 ± 0.6	0.62	0.82 ± 0.01	12.1	12.0	496 ± 7
$Ru(H_2L')_2(CN)_2$	3	581 ± 3	5.5 ± 0.1	0.63	0.80 ± 0.03	5.5	6.4	524 ± 4
$OsL_2(H_2L')^{2+}$	4	540 ± 10	7.7 ± 0.5	0.66	0.67 ± 0.03	7.5	7.6	487 ± 9
$RuL_2(H_2L')^{2+}$	4	532 ± 4	1.80 ± 0.05	0.62	0.45 ± 0.01	1.7	2.3	511 ± 7
$Os(H_2L')_3^{2+}$	3	514 ± 1	10.0 ± 0.2	0.69	0.73 ± 0.03	10.5	10.3	448 ± 3
$Ru(H_2L')_3^{2+}$	3	501 ± 2	3.7 ± 0.1	0.67	0.68 ± 0.03	3.8	4.7	468 ± 3

[a] Total number of experiments, each with a different electrode. [b] Fill factor for a representative resistance-corrected *J-E* curve [c] The predicted currents were standardized to the ELH bulb used using the average photocurrent for $Ru(H_2L')_2(NCS)_2$. 100 mW cm^{-2} is the power of the sun at AM 1.0.

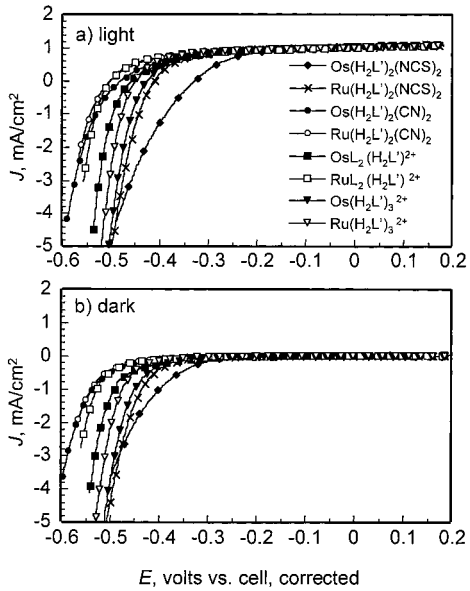

Figure 4. Corrected current density vs potential data for dyes on TiO_2 (a) (at a fixed short-circuit current density of 1 mA cm^{-2} and (b) in the dark.

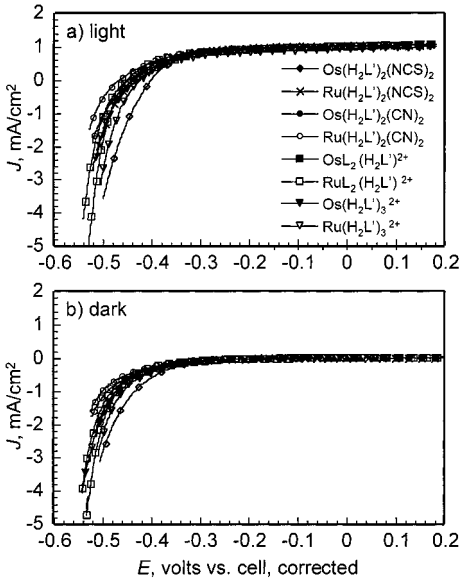

Figure 5. Corrected current density vs potential curves for TiO_2 electrodes having a low dye loading level (a) at a fixed short-circuit current density of 1 mA cm^{-2} and (b) in the dark.

Ru complexes, can also serve as efficient photosensitizers for TiO_2 in contact with the $CH_3CN-I_3^-/I^-$ electrolyte. The spectral response data of Figure 2 and Table 5 indicate that the Os complexes are indeed effective for this application. The external quantum yields for $Os(H_2L')_2(CN)_2$-coated TiO_2 electrodes are in excess of 0.8 and thus compare favorably to those of the analogous $Ru(H_2L')_2(CN)_2$-coated TiO_2 system. In addition, TiO_2 electrodes coated with the Os complexes showed enhanced absorption to the red relative to electrodes coated with their Ru analogues. Even TiO_2 electrodes coated with the Os complex that exhibited with the most positive excited-state redox potential $Os(H_2L')_3^{2+}$ were found to exhibit significant quantum yields for photocurrent flow in the $TiO_2/CH_3CN-I_3^-/I^-$ electrolyte with 50 mM pyridine and 20 mM pyridinium triflate. The relatively small differences in maximum quantum yield between all of these systems were shown to be likely due to engineering-related issues such as differences in coverage of the TiO_2 by the complexes as opposed to fundamental issues involved in the injection of electrons into the TiO_2 by the excited states of the various complexes studied herein.

The only significant discrepancy in this trend was observed for the $Os(H_2L')_2(NCS)_2$ complex. Although TiO_2 electrodes that had been coated with this complex showed enhanced external quantum yields in the red region of the spectrum relative to those coated with the analogous Ru complex, the maximum external quantum yield for $Os(H_2L')_2(NCS)_2$-coated TiO_2 was about a factor of 7 lower than that for $Ru(H_2L')_2(NCS)_2$-coated electrodes. The excited-state redox potential of this system is sufficiently negative that it is expected to inject electrons efficiently into the TiO_2, in a fashion analogous to that of the other complexes studied herein. Also, as discussed earlier, the low quantum yield cannot be ascribed to a low absorbance of these dye-coated electrodes since as much as 95% of the incoming light is adsorbed at 520 nm.

The low steady-state maximum external quantum yield in this system can be readily explained by the fact that the $Os(H_2L')_2(NCS)_2^{+/0}$ system has the most negative M(III)/M(II) ground-state redox potential of all the systems studied. Thus, this system is expected to have the highest ratio of its rate of recombination with electrons in TiO_2 relative to the rate of regeneration of the adsorbed M(II) species from the reaction of the adsorbed M(III) complex with I_3^-/I^- in the electrolyte. This high rate constant ratio allows the back reaction of electrons with Os(III) to compete with the regeneration of Os(II) through reaction with I^-. Evidence to support this hypothesis has been obtained from studying the dependence of the spectral response on the concentration of I^-. Although the other complexes showed essentially no dependence of their quantum yields on the I^- concentration, even at low light intensities, the observed photocurrent density for the $Os(H_2L')_2(NCS)_2$-coated TiO_2

TABLE 7: Photoelectrochemical Data for the Electrodes with Low Dye Coverage

complex	abs of electrode (at max of spectral response)	J_{sc} (mA cm$^{-2)}$ ELH bulb AM1.0	V_{oc} (mV) ELH bulb AM 1.0	ff resistance corrected *J-E* curve	V_{oc} (mV) at constant injection of 1 mA cm^{-2}
$Os(H_2L')_2(NCS)_2$	0.06	0.8	400	0.54	410
$Ru(H_2L')_2(NCS)_2$	0.07	2.3	510	0.64	470
$Os(H_2L')_2(CN)_2$	0.05	1.5	490	0.56	460
$Ru(H_2L')_2(CN)_2$	0.12	1.5	520	0.58	490
$OsL_2(H_2L')^{2+}$	0.16	2.7	500	0.54	470
$RuL_2(H_2L')^{2+}$	0.08	1	470	0.56	470
$Os(H_2L')_3^{2+}$	0.13	1.4	460	0.59	450
$Ru(H_2L')_3^{2+}$	0.19	0.9	450	0.62	460

TABLE 8: Photoelectrochemical Data vs [LiI] and/or [I_2]

	J_{sc}, ELH bulb, AM 1.0 (mA cm^{-2})				max external QY	
complex	0.5 M LiI, 0.04 M I_2	0.5 M LiI, 0.5 M $LiClO_4$, 0.04 M I_2	1.0 M LiI, 0.08 M I_2	2.5 M LiI, 0.04 M I_2	0.5 M LiI, 0.04 M I_2	2.5 M LiI, 0.04 M I_2
$Os(H_2L')_2(NCS)_2$	2.2	2.5	4.0	5.2	0.11	0.24
$Ru(H_2L')_2(NCS)_2$	11.1	11.0	11.0	10.8	0.77	0.79
$RuL_2(H_2L')^{2+}$	1.8	1.8	1.7			

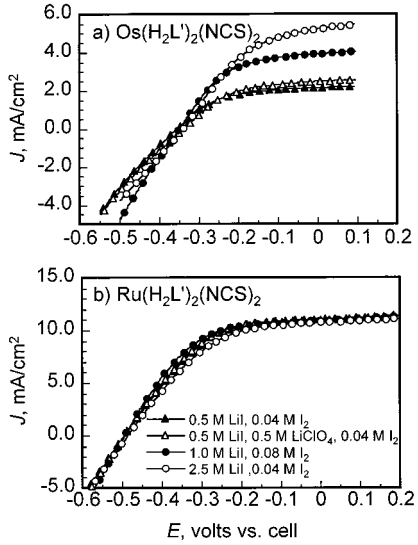

Figure 6. Current density vs potential behavior for TiO_2 electrodes coated with (a) $Os(H_2L')_2(NCS)_2$ and (b) $Ru(H_2L')_2(NCS)_2$ with various electrolytes. All electrolytes contained 0.050 M pyridine and 0.020 M pyridinium triflate.

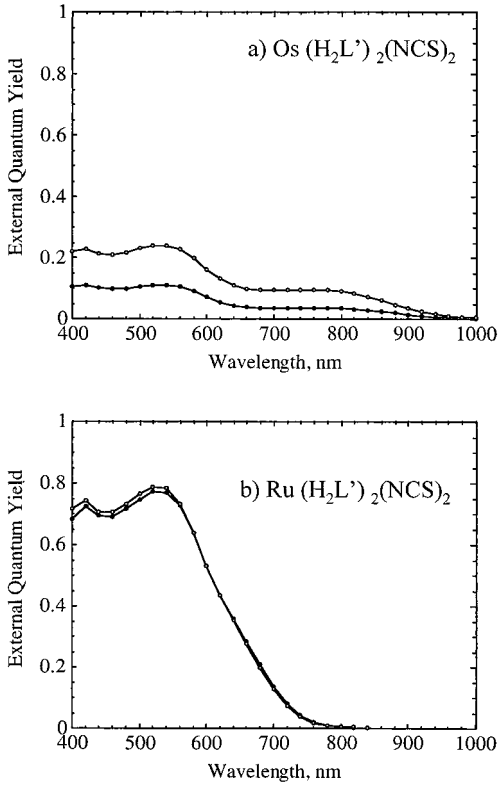

Figure 7. Spectral response data for TiO_2 electrodes coated with (a) $Os(H_2L')_2(NCS)_2$ and (b) $Ru(H_2L')_2(NCS)_2$. The closed circles (lower curves) indicate the behavior in CH_3CN/0.5 M LiI/0.04 M I_2 electrolyte. The open circles depict the behavior in CH_3CN/2.5 M LiI/0.04 M I_2. All electrolytes contained 0.050 M pyridine and 0.020 M pyridinium triflate.

electrodes increased when the concentration of I^- was increased from 0.5 to 1.0 M, keeping the redox potential of the electrolyte constant. This observation clearly implies that more rapid regeneration rates would allow the Os system to produce higher steady-state quantum yields than those obtained under the conditions used herein. This system is thus also expected to provide an efficient TiO_2 photosensitizer under optimized electrolyte/redox reagent conditions, although attaining such conditions will require either very high concentrations of I^- in order to increase the regeneration rate sufficiently, catalysis of this reaction, inhibition of the back electron transfer from the TiO_2 to the oxidized Os(III) complex, or use of another redox couple with more rapid regeneration kinetics but otherwise similar properties. Finally, further purification of this dye may also improve its performance as a photosensitizer.

The quantum yields measured in the spectral response experiments were obtained at relatively low irradiance levels, and there is some concern that these values might not be representative of the quantum yields under solar illumination intensities. A plot of J_{sc} vs light intensity for a $Ru(H_2L')_2(NCS)_2$-coated TiO_2 electrode was linear from $J_{sc} = 0.020$ mA cm^{-2} to $J_{sc} = 10$ mA cm^{-2}. Furthermore, if the spectral response is nearly independent of light intensity, the behavior of the dye-coated electrodes under solar or solar-simulated illumination can be predicted from the low-level quantum yield vs wavelength profile when convoluted with the spectral irradiance profile of the illumination source under the high light intensity conditions. The predicted J_{sc} value under ELH-type illumination can be obtained by the ratio of the integrated spectral response of the dye-coated TiO_2 electrodes to that of a calibrated Si photodiode. As seen in Table 6, the J_{sc} values predicted using this procedure are in good agreement with observations. These results also suggest that at photocurrents higher than a small threshold value, the short-circuit photocurrents are not affected by the surface electron concentration.

The photocurrents expected upon exposure of these cells to the NREL Global AM 1.5 solar spectral irradiance, at a total incident light intensity of 100 mW cm^{-2}, can be computed in a similar fashion. Two points are of main interest from analysis of these data (Table 6). First, the variation in predicted J_{sc} values arises mostly from the variation in the maximum external quantum yields. If the complexes are all normalized to the same maximum quantum yield value (Table 6), then it is clear that the Os complexes will outperform the Ru ones with respect to producing photocurrent under AM1.5 solar illumination. Second, even without such normalization, the TiO_2-coated $Os(H_2L')_2(CN)_2$ and $Os(H_2L')_3^{2+}$ systems at present provide comparable predicted J_{sc} values to the $RuL'_2(NCS)_2$-coated TiO_2 electrodes under our conditions. The Os complexes thus seem promising candidates for further optimization in operating photoelectrochemical cells for solar energy conversion applications based on their photocurrent and spectral response properties.

The simple model depicted in Scheme 1 fails to explain why the photocurrent at short circuit can be influenced by $[I^-]$ and not by surface electron concentration in the conduction band of TiO_2 for the $Os(H_2L')_2(NCS)_2$-coated electrodes. One possibility is that the back electron transfer to the dye occurs mainly from surface states and not from the conduction band electrons. In this model, the surface state electron concentration reaches a maximum constant value at a relatively small low light intensity. This model is consistent with the observation that photocurrents are nonlinear at very low light intensities, where the surface states may not be completely filled. This possibility is consistent with the recent work of Durrant and co-workers, who concluded from transient absorption spectroscopy that the recombination dynamics between TiO_2 and $Ru(H_2L')_2(NCS)_2$ and between TiO_2 and porphyrin-based sensitizers were dominated by the properties of TiO_2-based surface traps.[13b] Further experiments are needed to confirm this model in our system. The available data do, however, strongly suggest that the regeneration of adsorbed $Os(II)(H_2L')_2(NCS)_2$ by the redox couple does not compete with the back electron transfer to the dye in this system.

C. Current Density vs Potential Behavior. The other key property of concern is the photovoltage of the system. In our work, the performance of the devices has not been optimized through addition of surface passivating reagents, etc.; instead relatively uncomplicated, standard conditions of controlled proton activity, electrolyte concentration, etc., have been used in order to facilitate comparison between the performance of the various metal complex-coated TiO_2 electrodes in our studies. In a simple description of the operation of these photoelectrochemical cells, the open-circuit photovoltage should be the same for the various metal complexes, provided that the photocurrent density is constant for all electrode systems. This prediction is obtained because the dominant steady-state back reaction is thought to occur between electrons in the TiO_2 and I_3^- (I_2) in the electrolyte. If this is the case, a constant rate of injected carriers from the light should in turn produce a constant rate of back reaction, and thus a constant photovoltage at open-circuit (where the back reaction rate exactly offsets the light-driven forward current rate, which has been held constant experimentally), for the various systems of concern. As depicted in Table 7 and Figure 5, this behavior was indeed confirmed at low dye loadings for the various metal complexes studied in this work.

Interestingly, however, such behavior was not observed for TiO_2 electrodes that were coated with the higher loadings of dye that are needed to obtain the highest short-circuit photocurrent densities in an operating photoelectrochemical cell. Instead, as depicted in Table 6, the V_{oc} values at high dye loadings varied by over 100 mV even when the short-circuit current densities were held constant at $J_{sc} = 1.0$ mA cm^{-2}. As shown in Figure 4, this behavior was also seen in the dark $J-E$ properties of these electrodes, where the current density for reduction of I_3^- at a specific potential relative to short-circuit was observed to depend on the type of metal complex that was used to coat the TiO_2. In some cases, the dark currents were higher than those at an uncoated TiO_2 electrode, whereas in other cases, the dark reduction reaction was reduced by coating the TiO_2 with the metal complex.[39] Thus, in some cases adsorption of high levels of the metal complex appears to facilitate reduction of I_3^- in the solution, while in other cases, such levels of dye coverage appear to inhibit I_3^- reduction. At these potentials the metal complexes are all in the M(II) oxidation state, so they ought to be spectators in this reaction. However, the nature and coverage of the complex clearly play a more complicated role in determining the interfacial kinetics of the system than is produced by the simple working model for these electrode systems in the literature. Further study is clearly required in order to understand this behavior in detail. Given the relatively similar performance of the photocurrent density that is likely to be obtained from optimized systems from each of these metal complexes as described above, the variation in photovoltage is therefore likely to determine ultimately the relative utility of these various metal complexes in sensitizing TiO_2 for photoelectrochemical energy conversion applications.

V. Conclusions

Replacing the ruthenium metal center of polypyridyl complexes with osmium extended the light absorption and spectral response of nanocrystalline TiO_2 photoelectrodes to higher wavelength values without sacrificing significant photoelectrochemical energy conversion performance. The Os complexes thus seem very promising candidates for further optimization in operating photoelectrochemical cells for solar energy conversion applications. The ground-state potential of $Os(H_2L')_2(NCS)_2$ (0.4 V vs SCE) offers a lower limit for the ground-state redox potential of the dye in the current configuration of the electrochemical cell and redox couple. Finally, for electrodes with very low dye coverages, V_{oc} was mainly determined by the reduction of I_2, whereas a more complicated mechanism is apparently operative for electrodes having higher dye coverages.

Acknowledgment. Support for this project was provided by the U.S. Department of Energy, DE-FG07-96ER14725. M. Cass thanks Prof. John Burmeister of the University of Maryland for useful discussions on linkage isomerism in metal thiocyanate and metal isothiocyanate complexes, and Profs. H. Gray and J. Bercaw of Caltech are acknowledged for numerous helpful discussions. We are grateful to Dr. Andy Maverick at Louisiana State University for measuring the emission spectra of $Os(H_2L')_2(NCS)_2$. Geneviève Sauvé thanks FCAR (Fonds pour la Formation de Chercheurs et l'Aide à la Recherche, Québec, Canada) for a scholarship, and S.D. acknowledges the U.S. Global Change Fellowship Program for a postdoctoral fellowship. We also thank Kodak for a generous gift in support of studies of photoelectrochemistry at Caltech.

Supporting Information Available: ^1H NMR spectra of the complexes (aromatic region). This material is available free of charge via the Internet at http://pubs.acs.org.

References and Notes

(1) Tan, M. X.; Laibinis, P. E.; Nguyen, S. T.; Kesselman, J. M.; Stanton, C. E.; Lewis, N. S. *Prog. Inorg. Chem.* **1994**, *41*, 21.

(2) O'Regan, B.; Grätzel, M. *Nature (London)* **1991**, *353*, 737.

(3) Grätzel, M.; Kalyanasundaram, K. *Curr. Sci.* **1994**, *66*, 706.

(4) Nazeeruddin, M. K.; Kay, A.; Rodicio, I.; Humphry-Baker, R.; Müller, E.; Liska, P.; Vlachopoulos, N.; Grätzel, M. *J. Am. Chem. Soc.* **1993**, *115*, 6382.

(5) Heimer, T. A.; Bignozzi, C. A.; Meyer, G. J. *J. Phys. Chem.* **1993**, *97*, 11987.

(6) Argazzi, R.; Bignozzi, C. A.; Heimer, T. A.; Castellano, F. N.; Meyer, G. J. *Inorg. Chem.* **1994**, *33*, 5741.

(7) Nazeeruddin, M. K.; Müller, E.; Humphry-Baker, R.; Vlachopoulos, N.; Grätzel, M. *J. Chem. Soc., Dalton Trans.* **1997**, 4571.

(8) Nazeeruddin, M. K.; Péchy, P.; Grätzel, M. *Chem. Commun.* **1997**, *18*, 1705.

(9) a) Alebbi, M.; Bignozzi, C. A.; Heimer, T. A.; Hasselmann, G. M.; Meyer, G. J. *J. Phys. Chem. B* **1998**, *102*, 7577. (b) Farzad F.; Thompson, D. W.; Kelly, C. A.; Meyer, G. J. *J. Am. Chem. Soc.* **1999**, *121*, 5577. (c) Vrachnou, E.; Grätzel, M.; McEvoy, A. J. *J. Electroanal. Chem.* **1989**, *258*, 193. (d) Nazeeruddin, M. K.; Humphry-Baker, R.; Grätzel, M.; Murrer, B. A. *Chem. Commun.* **1998**, 719.

(10) Amadelli, R.; Argazzi, R.; Bignozzi, C. A.; Scandola, F. *J. Am. Chem. Soc.* **1990**, *112*, 7099.

(11) Kalyanasundaram, K. *Photochemistry of Polypyridine and Porphyrin Complexes*; Academic Press: San Diego, 1992; p 626.

(12) Hannappel, T.; Burfeindt, B.; Storck, W.; Willig, F. *J. Phys. Chem. B.* **1997**, *101*, 6799.

(13) a) Tachibana, Y.; Moser, J. E.; Grätzel, M.; Klug, D. R.; Durrant, J. R. *J. Phys. Chem.* **1996**, *100*, 20056. (b) Tachibana, Y.; Haque, S. A.; Mercer, I. P.; Durrant, J. R.; Klug, D. R. *J. Phys. Chem. B.;* **2000**; *104*, 1198.

(14) Rehm, J. M.; McLendon, G. L.; Nagasawa, Y.; Yoshihara, K.; Moser, J.; Grätzel, M. *J. Phys. Chem.* **1996**, *100*, 9577.

(15) Ferrere, S.; Gregg, B. A. *J. Am. Chem. Soc.* **1998**, *120*, 843.

(16) Eichberger, R.; Willig, F. *Chem. Phys.* **1990**, *141*, 159.

(17) Kalyanasundaram, K.; Nazeeruddin, M. K. *Chem. Phys. Lett.* **1992**, *193*, 292.

(18) Kober, E. M.; Caspar, J. V.; Sullivan, B. P.; Meyer, T. J. *Inorg. Chem.* **1988**, *27*, 4587.

(19) Bryant, G. M.; Fergusson, J. E.; Powell, K. J. *Aust. J. Chem.* **1971**, *24*, 257.

(20) Ethylene glycol was used as the solvent for this reaction, instead of dimethylformamide (DMF), to avoid the formation of carbonyl complexes. Such complexes can be observed in the infrared spectrum of the product, which displayed a prominent peak at 1720 cm^{-1} when DMF was used as the solvent.

(21) Sprintschnik, G.; Sprintschnik, H. W.; Kirch, P. P.; Whitten, D. G. *J. Am. Chem. Soc.* **1977**, *99*, 4947.

(22) Liska, P.; Vlachopoulos, N.; Nazeeruddin, M. K.; Comte, P.; Grätzel, M. *J. Am. Chem. Soc.* **1988**, *110*, 3686.

(23) a) Pomykal, K. E. Ph.D. Thesis, California Institute of Technology, 1997. (b) Sauve, G. Ph.D. Thesis, California Institute of Technology, 1999.

(24) Parks, G. A. *Chem. Rev.* **1965**, *65*, 177.

(25) Zhao, J.; Hidaka, H.; Takamura, A.; Pelizzetti, E.; Serpone, N. *Langmuir* **1993**, *9*, 1646.

(26) Kormann, C.; Bahnemann, D. W.; Hoffmann, M. R. *Environ. Sci. Technol.* **1991**, *25*, 494.

(27) Fajardo, A. M.; Lewis, N. S. *J. Phys. Chem. B* **1997**, *101*, 11136.

(28) Bard, A. J.; Faulkner, L. R. *Electrochemical Methods: Fundamentals and Applications*; Wiley: New York, 1980.

(29) Shklover, V.; Nazeeruddin, M.-K.; Zakeeruddin, S. M.; Barbé, C.; Kay, A.; Haibach, T.; Steurer, W.; Hermann, R.; Hissen, H.-U.; Grätzel, M. *Chem. Mater.* **1997**, *9*, 430.

(30) Murakoshi, K.; Kano, G.; Sada, Y.; Yanagida, S.; Miyazaki, H.; Matsumoto, M.; Murasawa, S. *J. Electroanal. Chem.* **1995**, *396*, 27.

(31) Kohle, O.; Ruile, S.; Grätzel, M. *Inorg. Chem.* **1996**, *35*, 4779.

(32) Howarth, O. W.; Richards, R. E.; Venanzi, L. M. *J. Chem. Soc.* **1964**, 3335.

(33) Pregosin, P. S.; Streit, H.; Venanzi, L. M. *Inorg. Chim. Acta* **1980**, *38*, 237.

(34) Herber, R. H.; Nan, G.; Potenza, J. A.; Schugar, H. J.; Bino, A. *Inorg. Chem.* **1989**, *28*, 938.

(35) Kargol, J. A.; Crecely, R. W.; Burmeister, J. L. *Inorg. Chem.* **1979**, *18*, 2532.

(36) Harris, D. C. *Quantitative Chemical Analysis*, 2nd ed.; W. H. Freeman and Co.: New York, 1987; p 818.

(37) Shklover, V.; Haibach, T.; Bolliger, B.; Hochstrasser, M.; Erbudak, M.; Nissen, H.-U.; Zakeeruddin, S. M.; Nazeeruddin, M. K.; Grätzel, M. *J. Solid State Chem.* **1997**, *132*, 60.

(38) Zakeeruddin, S. M.; Nazeeruddin, M. K.; Pechy, P.; Rotzinger, F. P.; Humphry-Baker, R.; Kalyanasundaram, K.; Grätzel, M. *Inorg. Chem.* **1997**, *36*, 5937.

(39) Stanley, A.; Matthews, D. *Aust. J. Chem.* **1995**, *48*, 1293.

(40) Fratiello, A.; Kubo-Anderson, V.; Adanalyan, A.; Bolanos, E. L.; Ortega, J. V.; Perrigan, R. D.; Saenz, L. *J. Solution Chem.* **1995**, *24*, 1249.

(41) Levy, G. C.; Lichter, R. L. *Nitrogen-15 Nuclear Magnetic Resonance Spectroscopy*; John Wiley & Sons: 1979.